

# Aberrant expression of agouti signaling protein (*ASIP*) as a cause of monogenic severe childhood obesity

Received: 8 September 2022

Accepted: 31 October 2022

Published online: 19 December 2022

 Check for updates

Elena Kempf<sup>1,14</sup>, Kathrin Landgraf<sup>1,14</sup>, Robert Stein<sup>1,2</sup>, Martha Hanschkow<sup>1</sup>, Anja Hilbert<sup>3</sup>, Rami Abou Jamra<sup>4</sup>, Paula Boczki<sup>1</sup>, Gunda Herberth<sup>5</sup>, Andreas Kühnapfel<sup>6</sup>, Yu-Hua Tseng<sup>7</sup>, Claudia Stäubert<sup>8</sup>, Torsten Schöneberg<sup>8</sup>, Peter Kühnen<sup>9</sup>, N. William Rayner<sup>10</sup>, Eleftheria Zeggini<sup>10,11</sup>, Wieland Kiess<sup>1,12</sup>, Matthias Blüher<sup>2,13</sup> & Antje Körner<sup>1,2,12</sup> ✉

Here we report a heterozygous tandem duplication at the *ASIP* (agouti signaling protein) gene locus causing ubiquitous, ectopic *ASIP* expression in a female patient with extreme childhood obesity. The mutation places *ASIP* under control of the ubiquitously active itchy E3 ubiquitin protein ligase promoter, driving the generation of *ASIP* in patient-derived native and induced pluripotent stem cells for all germ layers and hypothalamic-like neurons. The patient's phenotype of early-onset obesity, overgrowth, red hair and hyperinsulinemia is concordant with that of mutant mice ubiquitously expressing the homolog nonagouti. *ASIP* represses melanocyte-stimulating hormone-mediated activation as a melanocortin receptor antagonist, which might affect eating behavior, energy expenditure, adipocyte differentiation and pigmentation, as observed in the index patient. As the type of mutation escapes standard genetic screening algorithms, we rescreened the Leipzig Childhood Obesity cohort of 1,745 patients and identified four additional patients with the identical mutation, ectopic *ASIP* expression and a similar phenotype. Taken together, our data indicate that ubiquitous ectopic *ASIP* expression is likely a monogenic cause of human obesity.

Although there is doubtless a genetic component of common obesity, monogenic forms of human obesity are very rare<sup>1,2</sup>. Most of these single-gene defects affect the leptin–melanocortin 4 receptor (MC4R) pathway, which centrally regulates food intake and energy balance<sup>3,4</sup>. Detection of these<sup>5</sup> and new monogenic obesity traits<sup>6</sup> will not only improve our understanding of obesity mechanisms in humans but guide the development of new targeted pharmacotherapies increasingly available for affected patients<sup>2,7</sup>.

In a bottom-up approach, taking advantage of patient-derived adipose cells, we identified a potential new genetic cause of melanocortin obesity syndrome, phenocopying mouse and human proopiomelanocortin (*POMC*) deficiency and mouse *ASIP* mutants (so-called 'agouti mice').

## Case report

A girl of non-consanguineous parents of European ancestry first presented at the age of 1.9 years with overgrowth and severe obesity. From infancy onwards, she was reported to have a constant desire for food

A full list of affiliations appears at the end of the paper. ✉ e-mail: [antje.koerner@medizin.uni-leipzig.de](mailto:antje.koerner@medizin.uni-leipzig.de)

and developed progressive extreme obesity and tall stature (Fig. 1a,b) accompanied by first signs of severe hyperinsulinemia and hepatic steatosis in early childhood (Fig. 1c–h).

Both parents also suffer from obesity (Fig. 1i). The father has type 2 diabetes, hypertension and gout. In distinct phenotypic features (red hair color, pale skin and freckles), the girl resembles her father. Clinically relevant variants in genes related to monogenic obesity and other inherited diseases were excluded by whole exome sequencing. At the age of 12.4 years with a body mass index (BMI) of 47.6 kg m<sup>-2</sup> (BMI s.d. score (SDS) 3.8, weight 156 kg, height 181 cm and 3.34 SDS), she underwent bariatric surgery by sleeve gastrectomy leading to weight loss of 40 kg. She subsequently regained weight although metabolic improvement was retained (Fig. 1a–h).

During childhood, the patient reported being continuously hungry, except after eating very large amounts of food. She tried consciously to control food intake. At the age of 16 years, she scored high on the Eating Disorder Examination Questionnaire and the Dutch Eating Behavior Questionnaire, showing high cognitive restraint (>85th percentile) as well as extreme eating, weight and shape concerns (>95th percentile). She did not report binge eating, external (<5th percentile) or emotional eating (<25th percentile).

A clinical–psychological exploration noted remarkably low physical activity. Furthermore, indirect calorimetry revealed a reduced resting metabolic rate (1,660 kcal d<sup>-1</sup>, accounting for only 77.4% of the expected).

Hence, this phenotype of early-onset extreme obesity accompanied by tall stature, hypopigmentation and alterations in appetite and energy expenditure was suggestive for an underlying genetic or biological cause.

## Results

### Biological alterations and ectopic *ASIP* expression in adipose tissue

We obtained a sample of subcutaneous adipose tissue from the patient during bariatric surgery. Considering the severe overgrowth and obesity, we hypothesized that the adipose tissue-derived stromal vascular fraction (SVF) cells showed alterations in proliferative and/or adipogenic capacity. The patient's SVF cells showed pronounced adipocyte differentiation that was sustained in long-term cultivation compared to SVF cells from four age-matched controls with obesity (Supplementary Appendix, Supplementary Table 1 and Fig. 2a–d), whereas proliferation of the patient's SVF cells was not enhanced (Fig. 2e,f). We further found reduced mitochondrial maximum respiration, spare capacity and proton leak in the patient's SVF cells as proxies for reduced energy expenditure (Fig. 2g).

To identify potential molecular causes for the enhanced adipogenesis, we searched for differentially expressed genes in the patient's SVF cells compared to SVF cells from control children through transcriptome-wide analyses. Only one gene encoding *ASIP* was highly overexpressed in the index patient's cells (Fig. 3a).

We confirmed ectopic *ASIP* expression in several cell types, including isolated adipocytes, SVF cells and peripheral blood leukocytes, indicating ubiquitous expression in the patient (Fig. 3b–d, Supplementary Appendix and Supplementary Table 2). Concordantly, we found ectopic *ASIP* protein in SVF cell lysates and conditioned medium in the patient's cells. Inhibition of the secretory pathway lead to cellular retention of *ASIP*, confirming that the ectopically expressed *ASIP* is secreted<sup>8</sup> (Fig. 3e).

Physiologically, *ASIP* is expressed in the skin and regulates hair pigmentation through interaction with the melanocortin-1 receptor (MC1R). Ubiquitous expression of the murine *ASIP* homolog nonagouti in so-called agouti mice leads to yellow fur and obesity due to increased food intake, lipid storage in adipose tissue and reduced energy expenditure<sup>9–12</sup>. Hence, the concordant phenotype associated with ectopic expression of *ASIP* in our participants is likely a new monogenic obesity cause in humans.

### Chromosomal rearrangement causes aberrant ectopic

#### *ASIP* expression

Based on our finding of ectopic *ASIP* expression in the patient, we hypothesized an *ASIP* gene locus alteration. Genetic analyses including trio whole-genome sequencing (WGS), screen for copy-number variation (CNV) and cloning of the breakpoint sequence revealed a heterozygous 183-kbp tandem duplication on chromosome 20 encompassing the neighboring genes *ASIP* and itchy E3 ubiquitin protein ligase (*ITCH*) on the forward strand and adenosylhomocysteinase (*AHCY*) on the reverse strand (Fig. 4a). Additional clinically relevant variants or CNVs in genes related to obesity, such as *MC4R*, *POMC* and *LEPR*, were excluded by exome sequencing and a TruSight One Sequencing panel.

Both, *AHCY* and *ITCH* were not differentially regulated in transcriptome-wide analyses (Fig. 3a) and results from quantitative real-time PCR from SVF cells showed an approximately 1.5-fold increase in *AHCY* expression and no difference in *ITCH* expression (Extended Data Fig. 1a,b), whereas *ASIP* is overexpressed several hundredfold (Extended Data Fig. 1c). Similar results were obtained for peripheral blood leukocytes (Fig. 3d and Extended Data Fig. 1d,e). This is in line with the expectation from the genomic rearrangement resulting in three copies of the *AHCY* gene, no change in the number of *ITCH* coding exons and a switch of promoter usage driving *ASIP* gene expression by the ubiquitously active *ITCH* promoter.

As we saw a slight increase in *AHCY* expression, we investigated the effects of *AHCY* in more detail; however, experimental overexpression of *AHCY* in human Simpson–Golabi–Behmel syndrome (SGBS) preadipocytes<sup>13</sup> did not affect adipocyte differentiation or the expression of peroxisome proliferator-activated receptor- $\gamma$  (*PPARG*) as the master regulator of adipogenesis (Extended Data Fig. 1f). Hence, the main consequence of the chromosomal rearrangement mutation is ectopic *ASIP* expression.

Our index patient inherited the mutation from her father, as evidenced by ectopic *ASIP* expression in his peripheral blood leukocytes (Fig. 4b) and the presence of the duplication-specific *ITCH–ASIP* breakpoint sequence confirmed by WGS and breakpoint-specific quantitative polymerase chain reaction (qPCR) (Fig. 4c). The father harbors the same chromosomal rearrangement and according to self-reports had been taller and heavier than his peers from birth onwards. Starting at the age of 10 years, he engaged in competitive athletic sports and lost some weight. Nonetheless, he reported weighing 125 kg at the age of 18 years (BMI 36 kg m<sup>-2</sup>). He did not, however, score conspicuously on eating behavior questionnaires at the age of 52 years.

Both the patient and her father have red hair color and pale skin with freckles (Fig. 1i), which is another characteristic concordant with the yellow fur of the agouti mice ectopically expressing *ASIP* and is due to the action of *ASIP* as an antagonist at MC1R in the skin. We verified that neither the patient nor the father carries any genetic variant known to be associated with red hair, for example in *MC1R*<sup>14</sup> (Supplementary Appendix and Supplementary Table 3).

By 5' rapid amplification of complementary DNA ends and PCR (5'-RACE-PCR) and RNA-seq from peripheral blood and SVF cells, we demonstrated that the genetic rearrangement creates an *ITCH–ASIP* transcript consisting of the first two non-coding *ITCH* exons (5' untranslated region (UTR)) fused to the *ASIP* coding exons (Fig. 4d). This indicates that *ASIP* expression is under the control of the *ITCH* promoter. Concordant with the GTEx catalog, we found high *ASIP* gene expression in skin and low expression in other healthy human tissues (Fig. 4e). As *ITCH* is ubiquitously expressed in human tissues (Fig. 4f and concordant with the GTEx catalog), it explains the ubiquitous expression of *ASIP* in our patient.

We verified functional *ITCH–ASIP* interaction in luciferase reporter assays showing that a 2.8-kbp genomic region located upstream of *ITCH* exon 1 is capable of driving gene expression (Fig. 4g). Furthermore, we generated an artificial fusion gene by cloning the *ITCH–ASIP* fusion cDNA sequence under control of the 2.8-kbp *ITCH* promoter and

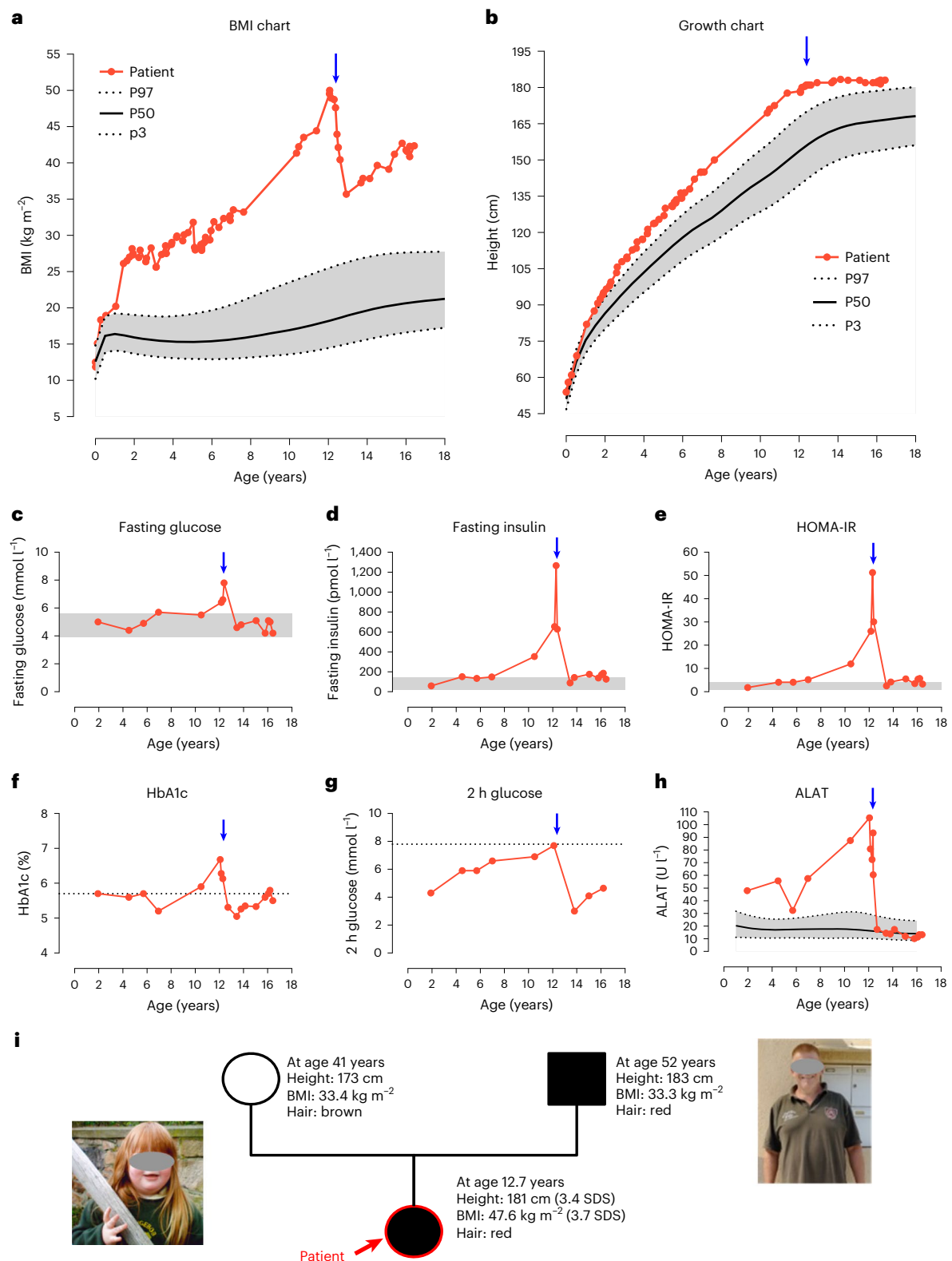


**Fig. 1 | Clinical characteristics of the index patient and her family. a, b**, Course of BMI (**a**) and height (**b**) of the patient (red dots) from birth to adolescence in relation to 3rd (P3), 50th (P50) and 97th (P97) sex-specific reference percentiles according to Kromeyer-Hauschild et al.<sup>40</sup>. Data from the patient were corrected for gestational age until the age of 2 years. **c–g**, Parameters of glucose metabolism with the respective reference ranges of either the local hospital laboratory depicted as gray areas or with prediabetes cut-offs according to the American Diabetes Association<sup>65</sup> indicated by a dotted line. **h**, Serum levels of liver enzyme alanine aminotransferase (ALAT) in comparison to the

values according to Bussler et al.<sup>66</sup> (shaded in gray). Blue arrows mark the time point of bariatric surgery at the age of 12.4 years. **i**, Pedigree of the family; females are indicated by circles, the father by a square. Individuals carrying the *AS1P* tandem duplication are indicated by black symbols, the open symbol indicates the mother not carrying the mutation. The index patient is indicated by a red arrow. Photographs present patient at age of 3.5 years and father at age 52 years. HbA1c, glycated hemoglobin; HOMA-IR, homeostatic model assessment for insulin resistance; 2 h glucose, glucose levels after 2 h of oral glucose tolerance testing.

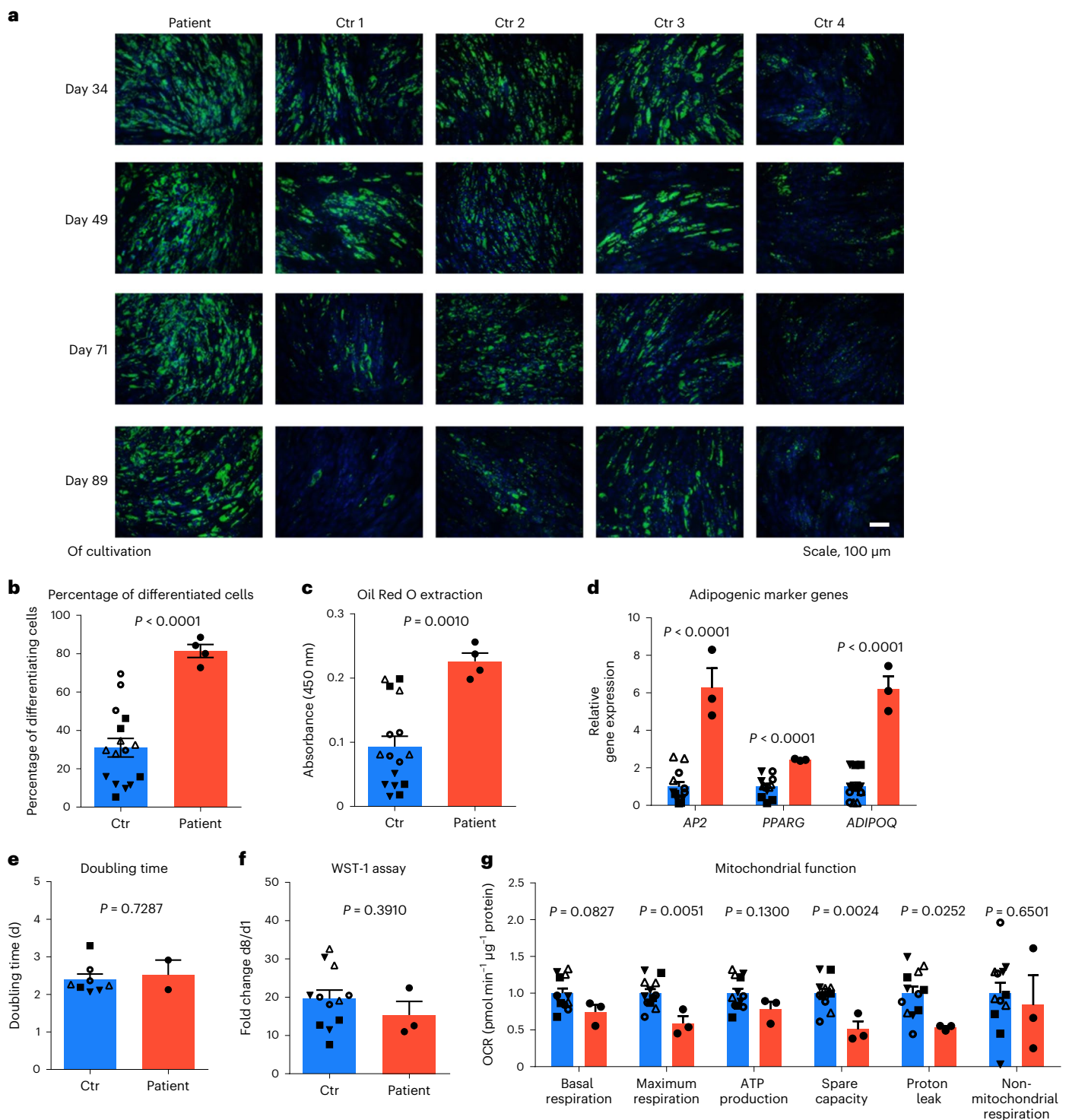


**Fig. 2 | Adipogenic and mitochondrial function of patient-derived adipose cells.** **a**, At indicated time points of cultivation, subcutaneous SVF cells from the patient and control (Ctr) children, all presenting with overweight or obesity ( $n = 4$ ; 3 females, 1 male), matched for age (mean age 13.8 years) were differentiated into adipocytes. Nuclei were stained with Hoechst (blue) and lipids with Nile red (green). **b**, Percentage of differentiated cells determined by cell counting. **c**, Using the same differentiated cells adipogenic capacity was quantified using Oil Red O. **d**, Relative expression of the adipogenic marker genes adipocyte protein 2 (*AP2*), peroxisome proliferator-activated receptor  $\gamma$  (*PPARG*) and adiponectin (*ADIPOQ*) in differentiated SVF cells from the patient and controls ( $n = 4$ ). The differentiation was examined over  $n = 3$  independent experiments (cells seeded for differentiation at days 65, 83 and 98 of cultivation).

Data are presented as fold change in relation to the controls. **e**, Doubling time of SVF cells from the patient and control children (Ctr,  $n = 4$ ) shown as mean with s.e. from  $n = 2$  experiments at day 49 and 71 of cultivation. **f**, Cell viability was assessed by WST-1 assay in  $n = 3$  experiments at day 49, 71 and 89 of cultivation. **g**, Mitochondrial function of SVF cells from the patient and controls ( $n = 4$ ) measured in  $n = 3$  independent experiments using the Seahorse Mito Stress Test kit. Data are presented as fold change in relation to the controls. The data points of each independent experiment are indicated for each individual (**b–g**). Bar plots represent the mean  $\pm$  s.e.m. All bar plots from controls are shown in blue and from the patient in red. Statistical significance was assessed using two-sided Student's *t*-test without adjustment of multiple comparisons.

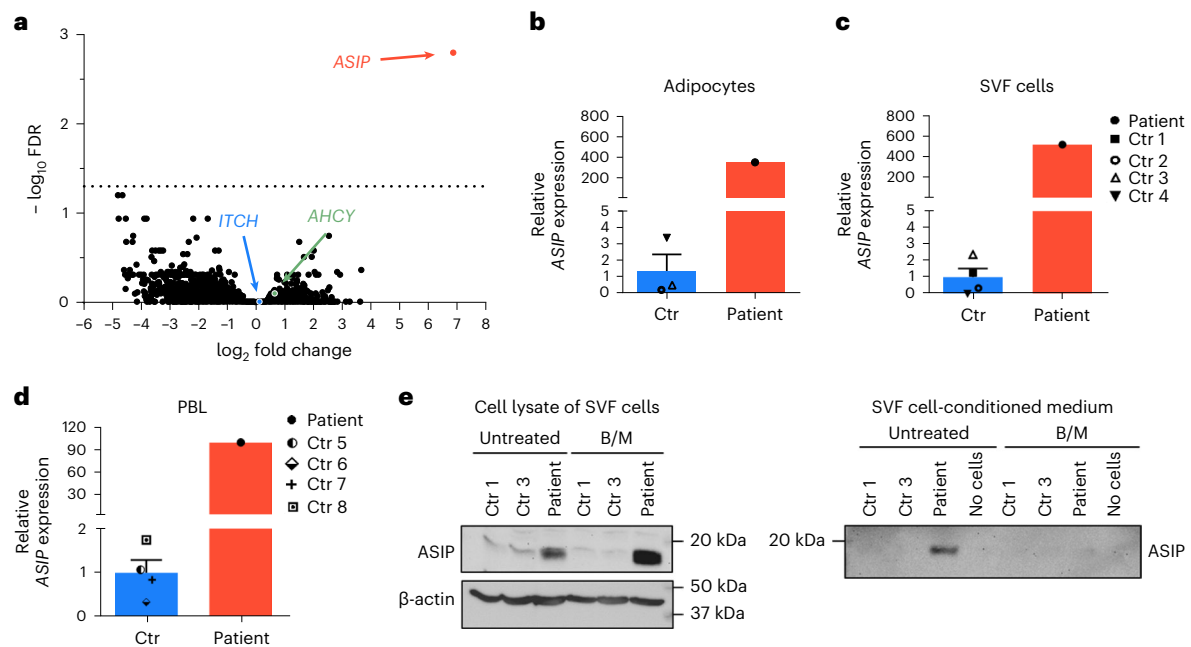


**Fig. 3 | Identification of ectopic *ASIP* expression in the patient.** **a**, Differentially expressed genes between undifferentiated SVF cells from the patient and control children (Ctr;  $n = 4$ ) presented as the  $\log_2$  fold change of gene expression across  $-\log_{10}$  false discovery rate (FDR). Similar results have been shown in a second independent experiment. **b–d**, *ASIP* gene expression levels are shown for adipocytes (**b**), SVF cells (**c**) and peripheral blood leukocytes (PBLs) (**d**). As PBL RNA samples from control children 1–4 were not available, measurements were performed in control children 5–8 (Supplementary Appendix and

Supplementary Table 1). **e**, *ASIP* protein was detected by immunoblotting in cell lysates and conditioned medium from untreated and brefeldin A and monensin (B/M)-treated SVF cells from the patient and two control children, 1 and 3. Similar results were obtained by a second independent experiment. Gene expression data shown in **b–d** were normalized to the expression of  $\beta$ -actin and TATA-box-binding protein. Bar plots represent mean  $\pm$  s.e.m. For **b–d** the fold changes in relation to mean of controls  $\pm$  s.e.m. are indicated. All bar plots from controls are shown in blue and from the patient in red.

confirmed increased production and secretion of ASIP protein (Fig. 4h) independent of the presence or absence of the *ITCH* 5'-UTR (Fig. 4i).

Thus, the chromosomal rearrangement positioning *ASIP* under the control of the *ITCH* promoter is the cause of the ubiquitous expression of *ASIP* in our patient and may thus be responsible for the clinical phenotype of our patient with early-onset extreme obesity, altered eating behavior, reduced energy expenditure and hypopigmentation.

### Retained ectopic *ASIP* expression in patient-derived iPSCs

To cause this agouti-like phenotype would require *ASIP* expression in central (hypothalamic) circuits. As these are naturally not directly accessible from patient samples and to provide further support that the genetic rearrangement in the patient causes ubiquitous *ASIP* expression in cells of all origins, we generated induced pluripotent stem cells (iPSCs) from patient-derived SVF cells and two control children. Ectopic *ASIP* expression persists in iPSCs from the patient compared to the controls (about 500-fold compared to controls; Fig. 5a), whereas *AHCY* is only slightly increased (about 1.25-fold) and *ITCH* is not differently expressed compared to controls (Extended Data Fig. 1g). We confirmed that *ASIP* protein is also secreted into the supernatant from patient iPSCs (Fig. 5b). We furthermore differentiated patient and control iPSCs into cells of the three germ layers mesoderm, ectoderm and endoderm and found ectopic *ASIP* expression in patient-derived iPSCs but not controls after differentiation in all germ layers (Fig. 5c). As the suspected mode of action is ectopic *ASIP* action in the hypothalamus, we went on and confirmed *ASIP* overexpression in patient-derived iPSCs differentiated into hypothalamic-like neurons via neuronal progenitor cells (Fig. 5d).

Finally, to experimentally confirm that *ASIP* indeed acts as an antagonist not only at MC1R but also at MC4R, we performed cAMP accumulation assays in CHO-K1 cells transiently transfected with human *MC1R* or *MC4R*. Increasing concentrations of *ASIP* cause a

reduction of basal activity of both human MC1R and MC4R activity with half-maximum inhibitory concentration ( $IC_{50}$ ) values of 4.4 nM and 16.9 nM, respectively. The natural ligand  $\alpha$ -melanocyte-stimulating hormone ( $\alpha$ -MSH) exerted agonistic activity at both receptors (MC1R half-maximum effective concentration ( $EC_{50}$ ) = 2.3 nM; MC4R  $EC_{50}$  = 10.6 nM), but presence of 100 nM *ASIP* caused a reduction of  $\alpha$ -MSH potency at both receptors, MC1R ( $EC_{50}$  = 65 nM) and MC4R ( $EC_{50}$  = 149 nM) (Fig. 5e).

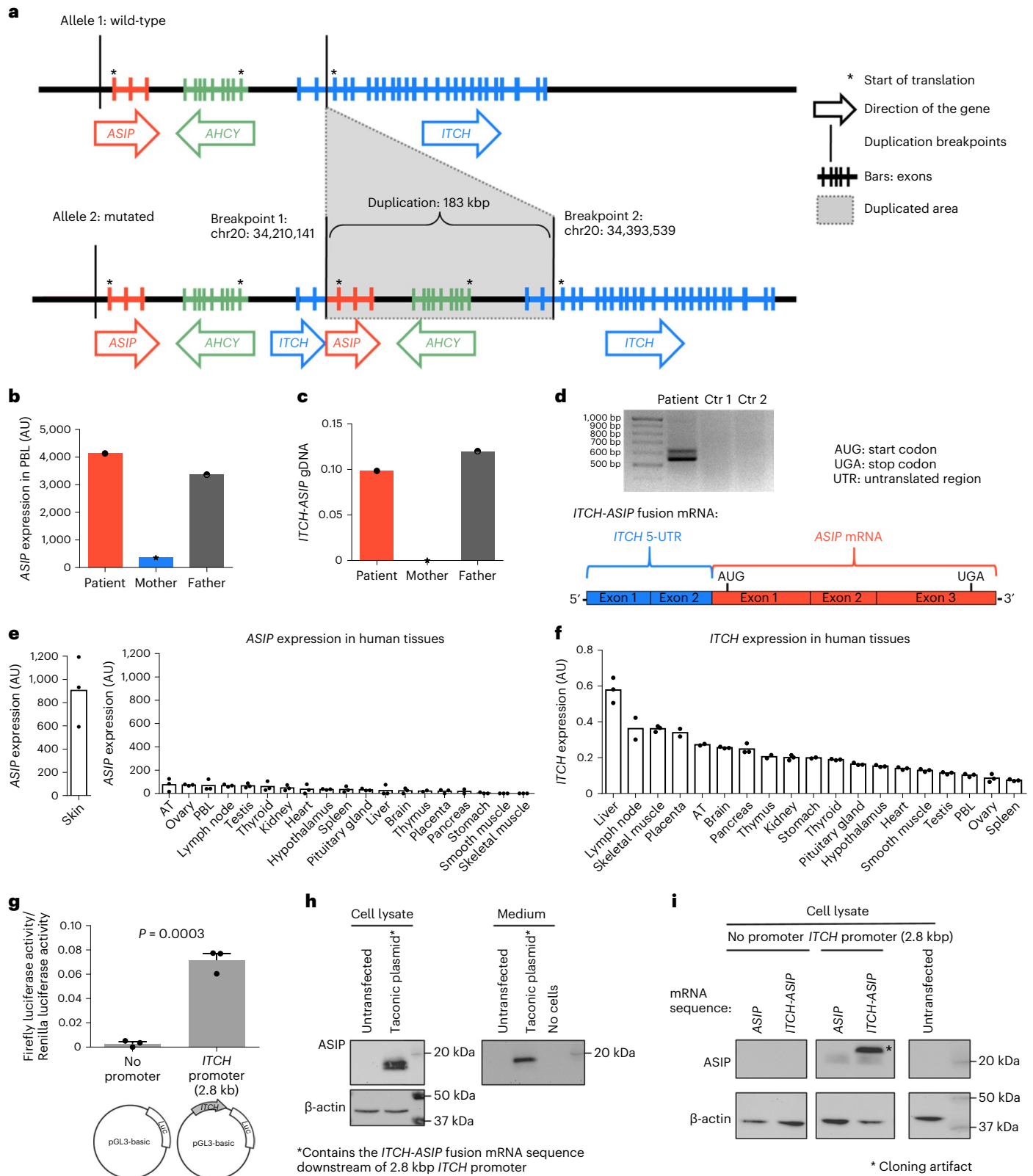
Hence, ubiquitous expression of the nonagouti homolog *ASIP* is found in patient-derived cells of all three germ layers supporting the hypothesis that ectopic *ASIP* antagonizes MC4R signaling in the hypothalamus of our patient, which would be required to affect processes related to eating behavior and energy expenditure and hence the obesity phenotype.

### Identification of additional patients with *ASIP* mutation

The type of genetic rearrangement is not readily detectable by standard genetic screening classically focusing on single-nucleotide variations. This may explain why there are no cases with detected *ASIP* mutations in the UK Biobank deposit or in the literature yet.

We screened a targeted 20 patients with a phenotype indicative of defects in the POMC pathway (extreme obesity and red hair color) for *ASIP* variants originally suspected but not diagnosed for *POMC* deficiency. However, we did not identify a patient with a similar *ITCH-ASIP* fusion (Fig. 6a).

Targeted screening of our Leipzig Childhood Obesity cohort ( $n = 1,745$ ) revealed four additional patients (three girls and one boy) carrying exactly the same mutation with the identical 5'*ITCH-ASIP* fusion as our index patient (Table 1). For three of them, RNA from peripheral blood was available and ectopic *ASIP* expression was confirmed (Fig. 6b). All four patients suffered from severe childhood obesity (Table 1). Compared to the obesity cohort, most patients carrying



the *ASIP* mutation have a BMI SDS and height SDS above the median (Fig. 6c). Notably, one of these patients has a twin brother, who does not harbor the mutation. Even though obesity is present in both brothers, they are discordant in the extent of obesity (>25 kg difference in body weight, difference BMI SDS 0.67; height difference of 8.8 cm, difference height SDS 1.18; all at the age of 11 years; Table 1).

To further support the link between the identified tandem duplication and childhood obesity, we screened healthy populational childhood cohorts ( $n = 2,051$ ). We performed power calculation assuming that the prevalence in the general pediatric population were identical to the one we observed in our obesity group (0.28%). According to this, with a power of 80% (significance level 0.05), screening

**Fig. 4 | Chromosomal rearrangement at the *ASIP* locus driving ectopic *ASIP* expression.** **a**, Schematic of the wild-type allele and the 183-kbp tandem duplication at the *ASIP*, *AHCY* and *ITCH* locus found in the patient. Locations of the breakpoints are presented according to the Dec. 2013 GRCh38/hg38 assembly. **b**, *ASIP* expression in PBLs in the patient, mother and father normalized to  $\beta$ -actin and *TBP*. **c**, Quantification of breakpoint-specific *ITCH-ASIP* fusion genomic DNA (gDNA) copy number in the patient, mother and father normalized to the copy number of  $\beta$ -actin gDNA. **d**, 5'-RACE-PCR from the patient and  $n = 2$  controls (Ctr). The lower band contained the *ITCH-ASIP* fusion mRNA sequence depicted below. The upper bands are incompletely spliced mRNA variants. **e, f**, *ASIP* (**e**) and *ITCH* (**f**) expression across human tissues normalized to expression of  $\beta$ -actin and *TBP*. Tissue RNA pooled from several individuals was purchased TakaraBio (three technical replicates). **g**, Luciferase assays in HEK293 cells transfected with vectors with or without a 2.8-kbp *ITCH* promoter sequence upstream of the luciferase (Luc) reporter gene. Firefly Luc activity

was normalized to *Renilla* Luc activity. Bar plots represent mean  $\pm$  s.e.m. of  $n = 3$  independent experiments. Statistical significance was assessed using two-sided Student's *t*-test. **h**, Immunoblot of *ASIP* in cell lysates and supernatants from HEK293 cells transfected with the Taconic plasmid containing the *ITCH-ASIP* mRNA sequence under control of the 2.8-kbp *ITCH* promoter. **i**, Immunoblot of *ASIP* in cell lysates and supernatants from HEK293 cells transfected with plasmids containing the physiological *ASIP* coding sequence or the *ITCH-ASIP* fusion mRNA sequence downstream of no promoter or the *ITCH* promoter. Asterisk indicates a cloning artifact as an additional band due to introduction of an additional translation start codon upstream of the mRNA sequence from the restriction enzyme *NcoI* (C'CATGG). This generated a functional open reading frame, exclusively for the *ITCH-ASIP* mRNA sequence, leading to an *ASIP* protein with additional N-terminal amino acids. The results shown in **h, i** were each confirmed by a second independent experiment.

of 2,154 probands should be sufficient to identify six carriers of the *ASIP* mutation (corresponding to 1 in 359). We did not find any in the healthy population cohort of 2,051 probands that we screened ( $P = 0.02$  with both Fisher's exact test and a chi-squared test with Monte Carlo simulation), further supporting that the tandem duplication is indeed associated with obesity.

Hence, identification of the additional, unrelated patients even in our local sample holds promise of detecting more patients with ubiquitous *ASIP* expression if genetic diagnostic algorithms are extended to chromosomal rearrangements.

## Discussion

We report an agouti-like human monogenic obesity trait that presents with extreme early-onset obesity, accelerated linear growth beyond what would be expected for children with obesity<sup>15</sup> and hypopigmentation. Based on experimental data from the analyses of patient-derived native and iPSCs, we identified ubiquitous ectopic *ASIP* expression due to chromosomal rearrangement as the likely cause of the phenotype (Fig. 7).

The identified tandem duplication leads to the generation of an ectopically expressed *ITCH-ASIP* fusion messenger RNA under control of the naturally ubiquitously active *ITCH* promoter and results in increased levels of secreted *ASIP* protein. In line with this, we found ectopic *ASIP* expression in several cell types of the patient (for example adipocytes and peripheral blood leukocytes). Even though desirable, we are not able to show ectopic *ASIP* expression directly in functional hypothalamic/brain circuits as we naturally do not have access to these patient tissues; however, patient-derived iPSCs differentiated into cells of all germ layers and further on into hypothalamic-like neurons, maintaining ectopic *ASIP* expression. These findings together with the fact that *ITCH* expression was detected in the brain and hypothalamus and that *ASIP* acts as an antagonist at the MC1R and MC4R, support that *ASIP* is ectopically expressed in the hypothalamus of the patient.

The murine *ASIP* homolog nonagouti is well known to be linked to obesity in rodents. The coding region of the human *ASIP* gene is 85%

homologous to the mouse gene<sup>16</sup> and there is high functional conservation<sup>17</sup>. Concordant with our patient, several rodent models with ubiquitous ectopic expression of nonagouti develop increased obesity, body length, yellow fur and hyperinsulinemia<sup>9,11,12</sup>. Notably, similar to that in naturally occurring agouti mice<sup>9</sup>, ectopic *ASIP* expression in our patient is caused by a gene rearrangement resulting in a change in promoter usage and hence ubiquitous and ectopic *ASIP* expression. Of note, there is a transgenic agouti mouse model, in which expression of the murine *ASIP* homolog is driven by the ubiquitously active human  $\beta$ -actin promoter, hence a very similar genetic constellation as we identified in our patient. These mice show overexpression of *ASIP* in the brain, leading to an obese phenotype with hyperphagia and hyperinsulinemia<sup>10</sup>.

Physiologically, the *ASIP* gene is expressed in hair follicles and antagonizes MC1R function on melanocytes and its ectopic expression, hence, causes yellow fur in mice. Although the physiological function of human *ASIP* does not seem to be entirely clear, we and others have shown it to be pharmacologically active and to antagonize the human melanocortin receptors<sup>17</sup>. Furthermore, genome-wide association studies revealed associations of variants at the *ASIP* locus with skin color, melanoma risk and red hair color, pointing toward a physiological function in hair and skin pigmentation similar to other mammals. Nevertheless, we did not find variants in *ASIP* or *MC1R* associated with red hair in our index patient, thus indicating that the pigmentation phenotype derives from the functional overexpression of *ASIP*. Apart from this, a study by Voisey et al. indicated that *ASIP* mRNA levels in adipocytes were sex-specifically correlated with BMI in adult human probands with opposite directions in men and women<sup>18</sup>. In contrast to this we found no or only spurious *ASIP* expression in subcutaneous adipose tissue samples of children from our Leipzig Adipose Tissue Childhood cohort<sup>19</sup> (Extended Data Fig. 2).

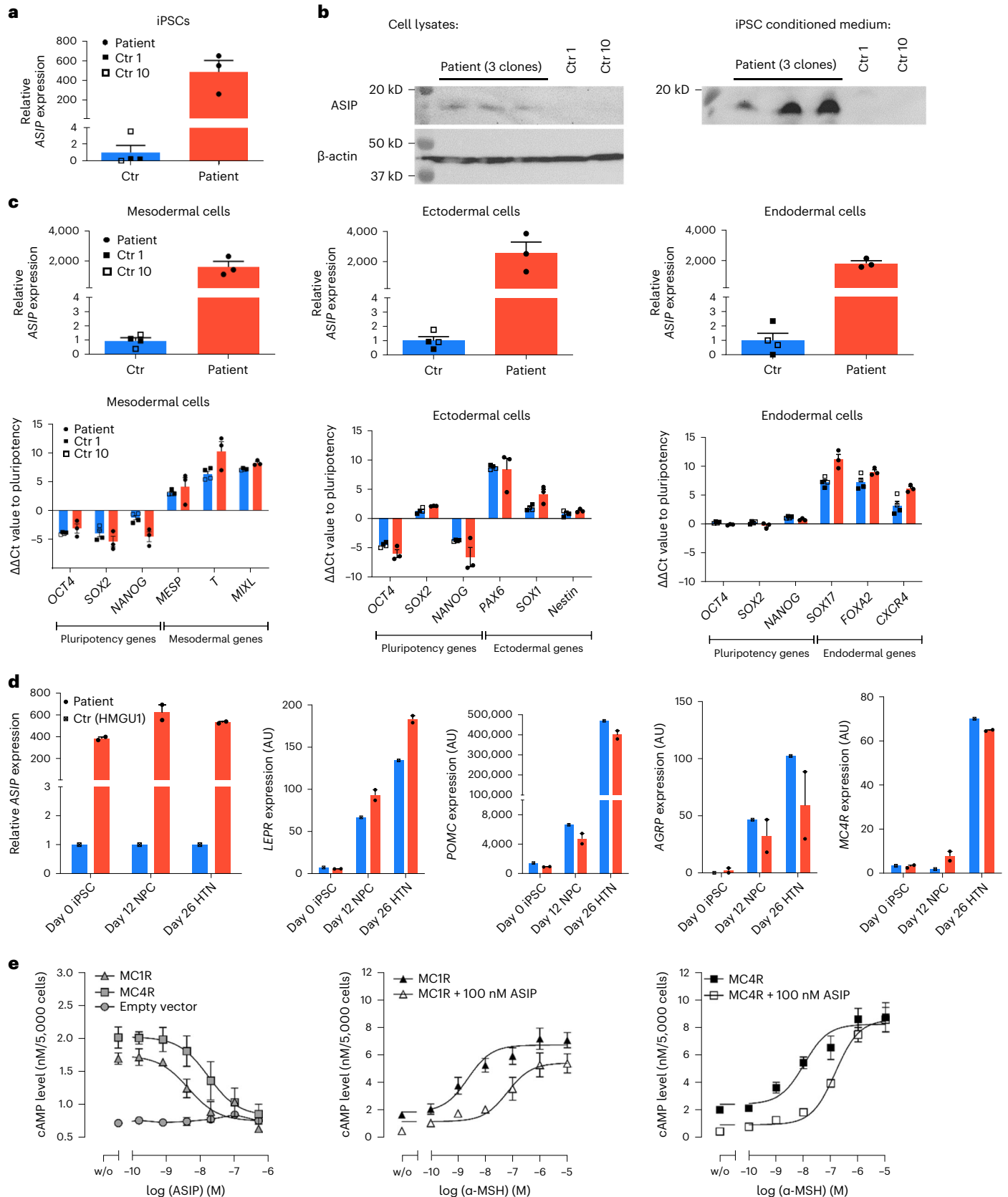
The obesity phenotype is explained by murine nonagouti/*ASIP* and human *ASIP* sharing structural similarity with agouti-related peptide<sup>20</sup>. When ectopically expressed in the hypothalamus, *ASIP* is hypothesized to interfere with the leptin-melanocortin axis by competitively

**Fig. 5 | Ectopic *ASIP* expression in patient-derived iPSCs persists during differentiation.** **a**, *ASIP* expression in SVF cell-derived iPSCs from  $n = 3$  clones (as biological independent samples) of the patient and  $n = 2$  clones from each control (Ctr) 1 and 10. **b**, Immunoblot of *ASIP* in cell lysates and supernatants from untreated iPSCs from the patient and the two control children. Similar results were obtained by a second independent experiment. **c**, Persisting *ASIP* expression in iPSCs of the patient ( $n = 3$  clones as biologically independent samples) but not of control children ( $n = 2$  clones each) differentiated into the three germ layers. Successful differentiation was confirmed by downregulation of the pluripotency markers *OCT4*, *SOX2* and *NANOG* and upregulation of germ-layer-specific markers (*MESP*, *T* and *MIXL* for mesoderm; *PAX6*, *SOX1* and *Nestin* for ectoderm; *SOX17*, *FOXA2* and *CXCR4* for endoderm). **d**, Persisting *ASIP* expression in patient-derived iPSCs ( $n = 2$  clones; red) but not HMGU1 iPSC

control cell line (blue) differentiated into hypothalamic-like neurons (HTNs) via neuronal progenitor cells (NPCs). Expression of hypothalamic marker genes *LEPR*, *POMC*, *AGRP* and *MC4R* confirmed successful differentiation. Gene expression levels were normalized to  $\beta$ -actin and TATA-box-binding protein. *ASIP* expression is presented as fold change in relation to the mean  $\pm$  s.e.m. of the controls. Relative expression levels of germ-layer marker genes were calculated by delta-delta Ct method normalized to  $\beta$ -actin. **e**, Antagonistic activity of *ASIP* in absence and presence of  $\alpha$ -MSH at human MC1R and MC4R. Basal cAMP levels concentration-dependently decreased in presence of increasing concentrations of *ASIP* (MC1R  $IC_{50} = 4.4$  nM; MC4R  $IC_{50} = 16.9$  nM).  $\alpha$ -MSH stimulates both MC1R ( $EC_{50} = 2.3$  nM) and MC4R ( $EC_{50} = 10.6$  nM). Presence of 100 nM *ASIP* lowers the potency of  $\alpha$ -MSH at MC1R ( $EC_{50} = 65$  nM) and MC4R ( $EC_{50} = 149$  nM). Data are mean  $\pm$  s.e.m. of  $n = 3$  independent experiments each performed in duplicate.

antagonizing the natural ligand  $\alpha$ -melanocyte-stimulating hormone at the MC4R and thereby centrally affecting food intake and energy expenditure; however, ubiquitous expression of *ASIP* in mice has been reported to result in rather moderate hyperphagia compared

to leptin- or leptin-receptor-deficient mice<sup>11</sup>. Similarly, our patient reported struggling with satiety before bariatric surgery and showed restrained eating, indicating a conscious counteracting of the hyperphagic drives that she sensed. Increased levels of incretins after





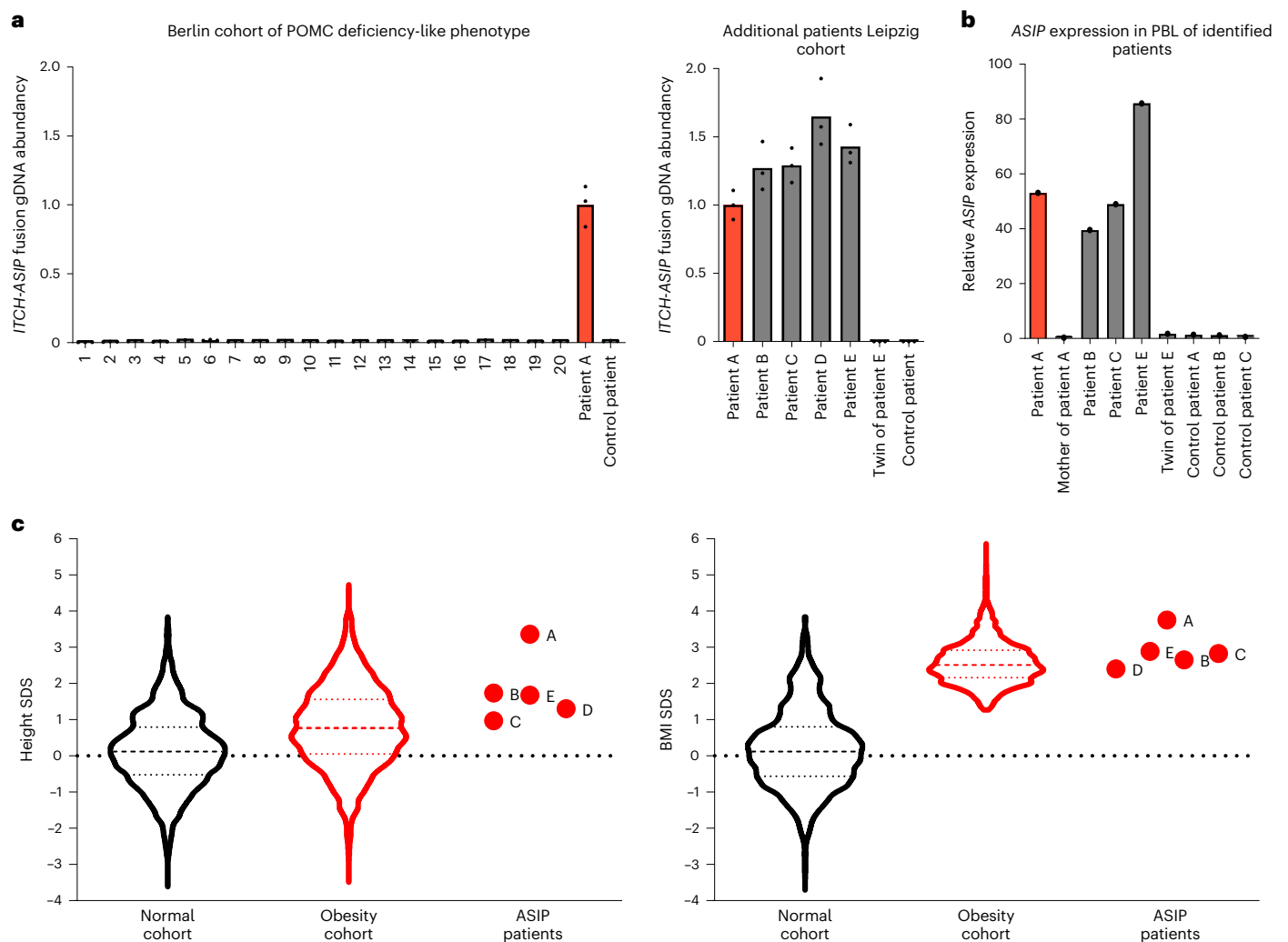


**Fig. 6 | Screening of obesity and populational cohorts for *ASIP* mutations.**

**a**, Cohort of patients originally suspected for *POMC* deficiency ( $n = 20$ ) from the University of Berlin and the Leipzig Childhood Obesity cohort were analyzed for copy numbers of the genomic *ITCH-ASIP* fusion sequence normalized to the copy numbers of  $\beta$ -actin. Patients A–E were identified with *ASIP* mutations. Samples from the index patient (patient A, red) were used as a positive control. A patient not harboring the *ASIP* mutation served as control. Data are given as fold change compared to patient A. **b**, *ASIP* gene expression in PBLs of patients normalized to  $\beta$ -actin and TATA-box-binding protein. Data are given as fold change to

control patients (consisting of the twin of patient E, the mother of patient A and three patients of the Leipzig Childhood Obesity cohort). **c**, Comparison of BMI SDS and height SDS of patients with *ASIP* mutation (as indicated) with healthy population ( $n = 1,868$ ; male  $n = 908$ ; mean age 10.0 years; open black) and with Leipzig Obesity Childhood cohort ( $n = 1,734$ ; male  $n = 861$ ; mean age 11.6 years; open red) shown as violin plots with median and quartiles indicated as dashed and dotted lines, respectively. Patients with *ASIP* mutation have significantly higher height SDS ( $P = 0.0419$  on two-sided Mann–Whitney  $U$ -test).

bariatric surgery may have affected neuronal MC4R signaling in the patient, further facilitating restrained eating<sup>21</sup>. Besides hyperphagia, other mechanisms may affect the development of obesity<sup>11,22</sup>. Agouti-related peptide in the hypothalamus affects energy expenditure<sup>23</sup>, locomotor activity<sup>24</sup> and sympathetic tone as well as shifting substrate utilization<sup>25</sup> in peripheral tissues. Ectopic *ASIP* may have analogous effects. Indeed, we observed reduced spontaneous physical activity in our patient and observed a decreased resting metabolic rate at the whole body and cellular level, which might at least partially contribute to the obesity phenotype. The father suffers from obesity, diabetes and has red hair. In childhood and adolescence he engaged intensely in competitive sports, which affects energy balance beneficially, but did not entirely prevent obesity. Variable phenotype–genotype concordance is also known in other monogenic causes of obesity, for example *MC4R* mutations<sup>26</sup>. It has been described that *MC4R* mutations and variants exhibit partial penetrance and age-dependent expressivity<sup>27</sup>. Of note, our index patient reported that her hair changed with age, from deep red (as a toddler) to more reddish and brown

(now as a young adult), which might indicate similar altered expressivity of the genotype–phenotype association. Although ectopic *ASIP* most likely promotes obesity primarily via central effects, ectopic *ASIP* may also contribute to obesity through peripheral effects as described for enhanced insulin secretion in the pancreas, leptin secretion from adipocytes, reduced lipolytic activity in adipocytes or regulation of adipogenic transcription factors<sup>22,28</sup> and it may even affect activation of brown AT<sup>29</sup>. In line with this, the patient showed hyperinsulinemia and her SVF cells differentiated better into adipocytes than SVF cells from controls, indicating additional peripheral obesity-related effects of ubiquitous *ASIP* expression. Potentially, primary hyperinsulinemia may also drive the linear overgrowth, as recently shown for epigenetically driven hyperinsulinemia causing gigantism in mice<sup>30</sup>.

Notably, although the patient experienced prominent weight regain after bariatric surgery, she showed sustained metabolic improvement. Apart from the described restrictive eating behavior of the patient and/or a potential sustained effect on incretin balance<sup>21</sup>, another potential explanation for this might be the young age of the

**Table 1 | Phenotype of patients carrying *ASIP* mutation**

Patient	A (index)	B	C	D	E	Fraternal twin of E
<b>Carrier of <i>ASIP</i> mutation</b>	Yes	Yes	Yes	Yes	Yes	No
<b><i>ASIP</i> overexpression in PBLs</b>	Yes	Yes	Yes	Not available	Yes	No
<b>Sex</b>	Female	Female	Female	Female	Male	Male
<b>Age (years)</b>	12.37	3.78	9.33	9.95	11.36	11.36
<b>Pubertal stage<sup>a</sup></b>	PH4, B4	PH1, B1	PH3, B2	PH1, B1	PH2, G1	PH2, G2
<b>Weight (kg)</b>	156.0	25.0	60.9	60.0	89.6	62.75
<b>Height (cm)</b>	181.0	109.5	143.9	149.8	160.7	151.9
<b>BMI SDS</b>	3.75	2.65	2.83	2.40	2.89	2.22
<b>Height SDS</b>	3.36	1.74	0.97	1.30	1.68	0.5
<b>Hair color</b>	Red	Red	Reddish	Reddish brown	Brown	Brown
<b>Hyperphagia</b>	Moderate	Severe	Moderate	Moderate	None	None
<b>Onset of overweight (obesity)</b>	1st YoL (1st YoL)	2nd YoL (2nd YoL)	2nd YoL (3rd YoL)	1st YoL (2nd YoL)	1st YoL (5th YoL)	1st YoL (5th YoL)
<b>Comorbidities</b>	Hyperinsulinemia, impaired glucose tolerance, hepatic steatosis, hyperuricemia	Hyperuricemia	Hyperinsulinemia, impaired glucose tolerance	Hyperinsulinemia, dyslipidemia	Bronchial asthma, dyslipidemia, global developmental delay	Global developmental delay

<sup>a</sup>Pubertal stages indicated by B, breast stage according to Tanner; G, genital stage (male) according to Tanner; and PH, pubic hair stage according to Tanner. YoL, year of life

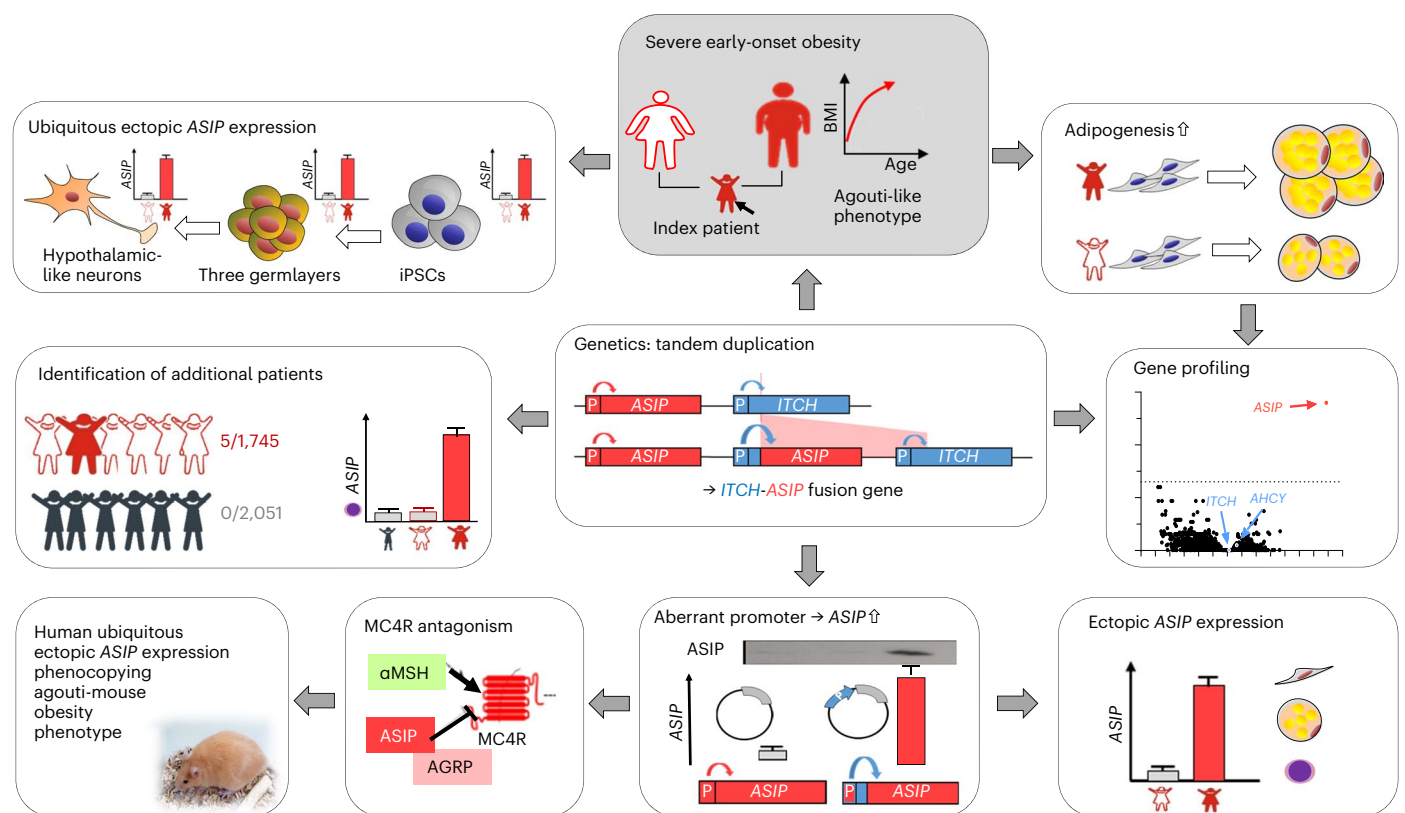


**Fig. 7 | Graphical summary.** Starting out from a case of a patient with severe early-onset obesity, accelerated linear growth, red hair and hyperinsulinemia (gray shaded box), we found enhanced adipogenesis of her SVF adipose-derived cells. Transcriptomic profiling identified aberrant *ASIP* expression, which is caused by chromosomal rearrangement with tandem duplication placing *ASIP* under the control of the *ITCH* promoter found in genetic profiling. Functionally verified aberrant promoter usage subsequently leads to ectopic *ASIP* expression

as verified in native and patient-derived iPSCs of the index patient. *ASIP* antagonizes *MC4R* signaling and thereby ubiquitous ectopic *ASIP* expression can induce a phenotype phenocopying the agouti mouse models. Cohort screening identified four additional patients carrying the same *ASIP* mutation, whereas none was identified in a population cohort. Carriers of the *ASIP* mutation are shown as red-shaded symbols, controls with obesity as white-shaded symbols and healthy children as gray symbols.

patient at surgery, as it has been shown previously that the benefit in remission of diabetes and hypertension from bariatric surgery was higher in adolescents compared to older patients<sup>31</sup>.

Likely there are more patients with undiagnosed ectopic *ASIP* expression, as the locus around *ASIP* is susceptible to genetic rearrangements<sup>32</sup>. In fact, patients with CNVs have been described

in publicly available databases (for example DECIPHER). These are mainly larger deletions of >1 Mbps. The CNV gain per se (with retained endogenous promoter linkage) is, however, not sufficient for ubiquitous and ectopic *ASIP* expression. This is fully dependent on the position of the breakpoints and rejoining points. The crucial consequence of the specific tandem duplication and the breakpoint/reinsertion point in our patient(s) is that one copy of *ASIP* is placed under control of the ubiquitous *ITCH* promoter and this results in ectopic *ASIP* expression.

Such gain-of-function mutations have been described in other species<sup>9,33,34</sup> and similar duplications resulting in an *ITCH-ASIP* fusion gene have been observed in sheep<sup>35</sup> and in quail<sup>36</sup>. The chromosomal rearrangement is, however, not readily detectable by routine sequencing approaches but requires techniques identifying CNVs. Only by targeted re-evaluation we were able to find four additional patients in a cohort of 1,745 children with overweight and obesity carrying the same genomic rearrangement as our index patient. That this is also associated with ectopic *ASIP* expression in blood cells further supports the finding of the tandem duplication causing the ectopic *ASIP* expression and the obese phenotype. In fact, the frequency of ~0.28% *ASIP* mutations in this pediatric obesity cohort may even reach the range of *MC4R* mutation prevalence, so far the most frequent monogenic obesity trait<sup>37</sup>. The screening of more patients to confirm this and to specify the phenotype of this monogenic trait caused by ectopic *ASIP* expression is pertinent, particularly as MCR agonists, such as setmelanotide as recently approved for deficiencies in components of the leptin–melanocortin signaling pathway<sup>7</sup>, provide a promising treatment option for these patients; however, concomitant stimulation of MC1R with setmelanotide causes skin pigmentation and may change melanoma risk<sup>38</sup>. Another treatment option might be glucagon-like peptide-1 receptor (GLP-1R) agonists as they have been shown to mediate weight loss in patients with *MC4R* mutations to a similar degree as in patients with polygenic obesity<sup>39</sup>; however, they would not target the underlying pathomechanisms at the MC4R. Agonists that are selective for MC4R or specifically target hypothalamic neurons would constitute a promising treatment option<sup>2</sup>.

In summary, we report that a genomic rearrangement leads to ubiquitous expression of *ASIP* in patients with severe early-onset obesity and overgrowth. This phenotype is concordant with mouse agouti obesity models ectopically expressing the homolog nonagouti/*ASIP*. Both, murine and human *ASIP* interfere with the melanocortin receptor signaling, which likely explains the obese phenotypes.

## Methods

### Oversight

The index patient and children of the control group were participants in the Leipzig Adipose Tissue Childhood<sup>19</sup> (NCT02208141, <https://clinicaltrials.gov/ct2/show/NCT02208141>, first registered August 2014) and the Leipzig Childhood Obesity (NCT04491344, <https://clinicaltrials.gov/ct2/show/NCT04491344>, first registered July 2020) cohorts<sup>15</sup>. Children from the age of 12 years and their guardians provided informed consent. The studies were approved by the Ethics Committee of the University of Leipzig (265/08, 007/04).

### Clinical and eating behavior data, energy expenditure

Height and weight were measured using calibrated devices to the nearest 1 mm and 0.1 kg, respectively. BMI and height were referenced to sex and age according to current guidelines<sup>40</sup> and were given as SDSs. Children were categorized into overweight ( $1.28 < \text{BMI SDS} \leq 1.88$ ) or obese (BMI SDS > 1.88) groups according to current national consensus guidelines<sup>41</sup>.

Blood parameters were measured by standard laboratory procedures in the Institute of Laboratory Medicine of the University of Leipzig.

Eating behavior was assessed by self-reports using validated questionnaires. The Eating Disorder Examination Questionnaire<sup>42,43</sup> assesses eating disorder psychopathology with subscales restraint,

eating, weight and shape concern and behavioral features (for example binge eating). Patient scores were compared to a reference population of 1,354 women <44 years of age<sup>44</sup> and father's scores to a reference population of 1,166 men aged 44–64 years (ref. <sup>44</sup>). The Dutch Eating Behavior Questionnaire<sup>45</sup> evaluates emotional eating, external eating and restraint using sum scores from Likert scales. Patient scores were compared to a reference population of 1,394 women between 14–94 years of age<sup>45</sup>.

Resting energy expenditure of the patient was examined at the age of 15 years following an overnight fast using an indirect calorimeter (Quark RMR, Cosmed Germany) according to the manufacturer's protocol. Expected metabolic rate was calculated according to her age, sex, height and body mass.

### Isolation and cultivation of SVF cells from adipose tissue

Subcutaneous AT samples were obtained from children undergoing bariatric or elective orthopedic surgery (Supplementary Table 1). SVF cells and adipocytes were isolated and preserved for later RNA isolation as previously described<sup>19,46</sup>. The remaining SVF cells were filtered through a nylon mesh with 30- $\mu\text{m}$  pore size. Erythrocytes were removed with erythrocyte lysis buffer (0.154 M NH<sub>4</sub>Cl (Sigma-Aldrich), 0.01 M KHCO<sub>3</sub> (Merck) and 0.1 mM EDTA (Sigma-Aldrich)). SVF cells were frozen in liquid nitrogen in Dulbecco's modified Eagle medium/Ham F-12 culture medium (DMEM/F-12) (Life Technologies) containing 10% fetal bovine serum (FBS) (Biochrom) and 10% dimethyl sulfoxide (DMSO) (Sigma-Aldrich). Cells were thawed and 24 h after seeding cells were washed three times with phosphate-buffered saline to select for adipocyte precursor cells via plastic adherence. Isolated SVF cells were cultivated in DMEM/Ham F-12 culture medium containing 10% FBS and 100 U penicillin and 0.1 mg ml<sup>-1</sup> streptomycin (Sigma-Aldrich) at 37 °C and 5% CO<sub>2</sub> and passaged every 3–4 d.

### Functional effects of *AHCY* overexpression

Human SGBS cells were kindly supplied by M. Wabitsch (University of Ulm) and cultured as previously described<sup>13</sup>.

pCMV plasmid transfections were performed with the Neon Transfection System 100  $\mu\text{l}$  kit (Invitrogen). The electroporation protocol was optimized to pulse voltage 1,300 V, pulse width 20 ms, pulse number 2 and a cell density of  $6 \times 10^6$  cells ml<sup>-1</sup>. SGBS cells were transfected with 5  $\mu\text{g}$  of pCMV-AHCY plasmid, for *AHCY* overexpression or the pCMV-Entry (both oriGene) as a control, per  $1 \times 10^6$  cells. After electroporation, 500,000 cells per well were seeded in a 12-well format for differentiation assay.

### Proliferation assay

For assessing proliferation, 500 SVF cells were seeded at day 49, 71 and 89 of cultivation per well in 96-well plates in five replicates and cultivated for 8 d. After 1 and 8 d, cell viability was assessed by WST-1 assay (Roche, Applied Bioscience) according to the manufacturer's protocol. Afterwards, cells were fixed, stained with Hoechst 33342 (Sigma-Aldrich) and counted by microscope. Doubling time (days) between d1 and d8 was calculated as  $(\text{duration (8 d)} \times \log_{10}(2)) / (\log_{10}(\text{cell number per image d1}) - \log_{10}(\text{cell number per image d8}))$ <sup>47</sup>.

### Differentiation assay

For assessing adipogenic capacity, in technical triplicates 30,000 SVF cells at day 34, 49, 71 and 89 of cultivation were seeded per well in a 48-well dish or transfected SGBS cells in a 12-well format were used. Cells were grown to confluence for 24 to 48 h and differentiated according to the Poietics human adipose-derived stem cell-adipogenesis protocol (Lonza) for 8 d (SVF cells) or 10 d (transfected SGBS cells).

Differentiated cells were fixed with Roti-Histofix 4% (Carl Roth), double-stained with 10  $\mu\text{g ml}^{-1}$  Nile red (Sigma-Aldrich) and 40  $\mu\text{g ml}^{-1}$  Hoechst 33342 (Sigma-Aldrich). The percentage of differentiated cells is given as mean from  $n = 3$  technical replicates calculated as (number of

counted differentiated cell per microscopic image) / (total number of cells per image). A cell was defined to be differentiated when containing at least two lipid droplets. Additionally, the cells were stained with Oil Red O (Sigma-Aldrich) solution (0.3% in 60% isopropanol) for 15 min and washed with H<sub>2</sub>O. Oil Red O was extracted with isopropanol and absorption was measured at 540 nm.

### Bioenergetic profiling

Mitochondrial function was assessed using the Seahorse XFe24 Analyzer (Agilent Technologies) and the XF Cell Mito Stress Test kit (Agilent Technologies) using concentrations of 2  $\mu$ M oligomycin, 3  $\mu$ M carbonyl cyanide-4 (trifluoromethoxy) phenylhydrazone and 1  $\mu$ M rotenone/antimycin A. A total of 15,000 SVF cells from the patient or control children were seeded into gelatin-coated wells of XFe24-plates in 3–4 technical replicates. Measurements were performed 48 h post-transfection using XF Base Medium (Agilent Technologies) containing 2 mM pyruvate (Sigma-Aldrich), 10 mM glucose (Sigma-Aldrich) and 2 mM glutamine (Sigma-Aldrich). Results were normalized to total protein per well ( $\mu$ g) by lysing the cells in 30  $\mu$ l 50 mM NaCl solution (Carl Roth) with subsequent protein quantification using the Pierce BCA Protein Assay kit (Thermo Fisher Scientific).

### Isolation of nucleic acids

RNA was isolated from SVF cells and reverse-transcribed as previously described<sup>48</sup>. From blood, RNA was extracted using the PAX-gene Blood RNA Tubes protocol (PreAnalytics). RNA from different human tissues pooled from several individuals were obtained from Clontech-TakaraBio. Genomic DNA was extracted from EDTA blood samples using the QIAamp DNA Blood Mini kit (QIAGEN).

### Transcriptome-wide analyses

Gene expression was measured using a HumanHT-12 v4 BeadChip array (Illumina). The R package limma was used to perform preprocessing (that is, background correction and quantile normalization) and differential gene expression analyses<sup>49</sup> (<https://doi.org/10.5281/zenodo.7223530>). Fold changes were log<sub>2</sub>-transformed and *P* values were adjusted for multiple testing using the Benjamini–Hochberg procedure (FDR).

### qRT-PCR

Quantitative real-time PCR (qRT-PCR) was performed as previously described<sup>48</sup> using the QuantStudio3 Real-Time PCR System (Applied Biosystems) with the qPCR Master Mix Plus - Low ROX (Eurogentec) or the Takyon Low ROX Probe Master Mix dTTP Blue (Eurogentec). Gene expression was quantified using a standard curve of serial dilutions from a linearized plasmid containing the target sequence or from a reference sample. Gene expressions were normalized to the expression of  $\beta$ -actin and TATA-box-binding protein. For measurement of *ASIP* expression in subcutaneous adipose tissue samples from the Leipzig Adipose Tissue Childhood cohort hypoxanthine-guanine-phosphoribosyltransferase was used as a third reference gene. Supplementary Appendix and Supplementary Table 4 lists all sequences of primers and probes and TaqMan Gene Expression Assays (Thermo Fisher Scientific) used for qRT-PCR.

### 5'-RACE-PCR

5'-RACE-PCR was performed from peripheral blood RNA using the SMARTer RACE cDNA Amplification kit (Clontech Laboratories) using primers in Supplementary Appendix and Supplementary Table 5.

### RNA-seq and transcript analyses

RNA was isolated from SVF cells of the patient and control children 1–4 as well as from peripheral blood mononuclear cells of the patient and control 9 using TRI REAGENT (Sigma-Aldrich). RNA quantity was measured with a spectrometer (Nanodrop ND 1000). We included only RNA samples with RIN values >8 analyzed on the Agilent 2100 bioanalyzer

using the RNA 6000 Nano Chip (Agilent Technologies). Indexed cDNA libraries were generated using TruSeq RNA Sample Preparation kits v2 (Illumina). The average library size was 300 bp as determined on the Agilent 2100 Bioanalyzer with DNA 1000 Chips. The libraries were sequenced on the Illumina HiScanSQ Sequencing System (Macrogen).

Reads were mapped to the reference human genome (GRCh38.p13, INSDC Assembly GCA\_000001405.28, Dec 2013) using TopHat (v.2.1.1)<sup>50</sup>. After indexing with samtools (v.1.9)<sup>51</sup> the mapped reads were assembled to transcripts and quantified by StringTie (v.2.1.3b)<sup>52,53</sup>. For TopHat, we used the 'default' parameters. StringTie parameters 'read coverage' (-c), 'transcript length' (-m) and 'bases on both sides of a junction a spliced read has to cover' (-a) were set to minimal values. The parameter 'fraction of most abundant transcript at one locus' (-f) was lowered from default (0.01) to 0 as correction for artifacts and incompletely processed mRNA with a 1% cutoff was performed after the comparative analysis. For all other StringTie parameters default values were used. Assembled transcripts were inspected with the Integrated Genome Viewer (Broad Institute)<sup>54,55</sup> and samples showing a visible 3' bias due to oligonucleotide-dT/poly-A primer selection were not included.

Due to small sizes of the exons of *ITCH* and *ASIP* coverage, analyses of single exons were not possible. Instead, a de novo assembly of *ITCH* and *ASIP* transcripts was performed using StringTie. Three new transcript variants occurred containing only the first two annotated exons of *ITCH*. The fragments per kilo base per million mapped reads for these variants and also of the *ASIP* and *AHCY* transcripts were compared between the patient and the controls.

### Genomic and genetic analyses

Trio WGS and bioinformatic analyses were performed at the DRESDEN-concept Genome Center. After ultrasonic shearing of 800 ng gDNA (LE220, Covaris) the DNA library preparation was performed using the Kapa HyperPlus kit (Roche) according the manufacturer's instructions. After ligation with uniquely dual indexed adaptors (IDT), non-ligated adaptors were removed by adding XP beads (Beckmann Coulter) in a ratio of 1:0.9. The DNA libraries were then size selected with XP beads to an average insert size of 300 bp and quantified by qPCR (LightCycler 480, Roche) and the Fragment Analyzer (Agilent). Libraries were sequenced paired end 2  $\times$  150 bp to a coverage >38 $\times$  on a NovaSeq 6000 (Illumina). Bioinformatic analysis was performed using the Illumina DRAGEN pipeline (07.021.595.3.7.5).

The TruSight One Sequencing panel was performed after enrichment with Nextera DNA Flex Pre-Enrichment LibraryPrep and Enrichment, IDT for Illumina Nextera UD Indexes and the NextSeq 500/550 High Output v2 kit (300 cycles) using the Illumina NextSeq 500/550. Data were analyzed using the software Varvis and Varfeed (Limbus). All analyses were performed according to American College of Medical Genetics and Genomics criteria.

Molecular karyotyping of genomic DNA was performed by array comparative genomic hybridization using the Infinium CytoSNP-850K v.1.2 BeadChip (Illumina) and analyzed using BlueFuse Multi (v.4.4).

### Luciferase reporter and expression assays

DNA sequences were cloned according to the TOPO TA Cloning kit, Dual Promoter protocol and confirmed by sequencing by the Core Unit for DNA technologies of the University of Leipzig. Primers used for cloning are indicated in Supplementary Appendix and Supplementary Table 5.

For luciferase assays the *ITCH* promoter was inserted upstream the luciferase reporter gene into the pGL3-Basic vector using the restriction enzymes *SacI* and *XhoI*.

For generation of modified pGL3-Basic expression vectors containing the *ASIP* or the *ITCH-ASIP* coding sequence under control of *ITCH* or no promoter, the luciferase reporter gene was cut out of the pGL3-Basic vector using *NcoI* and *XbaI* and the cloned mRNA sequences were inserted. Subsequently, the promoter sequence of *ITCH* was inserted into those vectors using the restriction enzymes *SacI* and *XhoI*.

A second independent expression vector containing the coding sequence of *ASIP* fused to the 5' UTR of *ITCH* under control of the *ITCH* promoter (2.8 kbp upstream of transcription start) was generated by Taconic Bioscience, as shown in Supplementary Appendix and Supplementary Fig. 1.

For luciferase reporter assays, 500,000 human embryo kidney cell line 293 (HEK293) (Sigma-Aldrich, ECACC 85120602) cells were seeded per well (six-well dish plate) and were co-transfected 24 h post-seeding with 1 µg of pGL3-Basic plasmids containing the firefly luciferase reporter under control of a 2,868 bp *ITCH* promoter sequence or no promoter and 50 ng of pRL-CMV control plasmid containing the luciferase gene from *Renilla reniformis* using 3 µl Fugene HD transfection reagent (Promega). Luciferase activities were measured using the Dual-Luciferase Reporter Assay System (Promega) according to the manufacturer's protocol 48 h post-transfection using a CLARIOstar plate reader (BMG Labtech). Experiments were performed in technical duplicates. For normalization, the sum of firefly luciferase signal was divided by the sum of *Renilla* luciferase signal.

### Generation and differentiation of patient-derived iPSCs

The generation of iPSCs from SVF cells isolated from adipose tissue of the patient and two control patients, 1 and 10, was performed by the iPSC Core Facility, Institute of Stem Cell Research, Helmholtz Zentrum Munchen. Pluripotency was confirmed by staining of OCT4, SOX2, LIN28 and NANOG<sup>56</sup>. The iPSCs were cultivated on Geltrex (Thermo Fisher Scientific)-coated cell culture plates in mTeSR1 medium (Stem Cell Technologies) at 37 °C and 5% CO<sub>2</sub>.

Characterization of the pluripotency of patient-derived iPSCs was performed as monolayers by directed differentiation into the ectodermal<sup>57</sup>, mesodermal<sup>58</sup> and endodermal<sup>59</sup> germ layers for a period of 5 d and subsequent qRT-PCR analyses of marker genes for each of the germ layers, as previously described<sup>56</sup>. Relative expression levels were calculated using the delta-delta Ct method normalized to β-actin.

Differentiation of patient-obtained iPSCs and the HMGU1 control iPSC line (kindly supplied by iPSC Core Facility, Institute of Stem Cell Research, Helmholtz Zentrum Munchen) into HTNs followed the previously described protocol of Wang et al.<sup>60</sup>. For generating hypothalamic NPCs, 500,000 iPSCs per well were cultured on Geltrex-coated 12-well-plates as described in the protocol and collected at day 12. For further differentiation, 300,000 single cells per well were plated on poly-L-ornithine- (0.01%, Sigma-Aldrich) and laminin-coated (4 µg ml<sup>-1</sup>; Thermo Fisher Scientific) 24-well plates. After cells had attached to the plate, the medium was replaced with N2 medium with B27 and 10 µM DAPT. Four days later, the medium was changed to N2 medium with B27 and 20 ng ml<sup>-1</sup> BDNF (R&D) and cells were cultured until day 26.

### Immunoblotting

For analysis of ASIP protein secretion 800,000 SVF cells were seeded on 15-cm plates, cells and supernatants were collected after 24 h of incubation with the secretory pathways inhibitors 5 µg ml<sup>-1</sup> brefeldin A (in DMSO; BioLegend) and 2 µM monensin (in 70% ethanol; BioLegend) or the control medium containing the same volume of DMSO and ethanol.

For analysis of ASIP protein generation from the fusion construct, 600,000 HEK cells were seeded per six-well dish and transfected 24 h later with 2 µg plasmid using 8 µl using Fugene HD transfection reagent (Promega) per well. Medium was changed 24 h after transfection. Cells and supernatants were collected 48 h after medium change for immunoblotting.

For the analysis of ASIP protein generation and secretion in the iPSC lines, cells were grown in six-well-plates to confluence before the medium was changed to 1 ml knockout DMEM with 1× MEM NEAA, 1× β-mercaptoethanol, 0.1% BSA (Serva), 100 U penicillin, 0.1 mg ml<sup>-1</sup> streptomycin and 2 mM glutamine. After 24 h, cells and supernatants were collected for immunoblotting.

Conditioned medium was centrifuged for 5 min at 800g and the supernatant lyophilized and re-suspended in H<sub>2</sub>O for receiving 10× concentrated medium. Cells were lysed in RIPA lysis buffer (50 mM Tris pH 7.5, 150 mM NaCl, 1% Triton X-100 and 0.1% SDS, with cComplete Mini Protease Inhibitor Cocktail Tablets; Roche, Sigma-Aldrich) with additional break-up via QiaShredder Homogenizer Columns (QIAGEN). The protein concentration of cell lysates was measured using the Pierce BCA Protein Assay kit (Thermo Fisher Scientific). Equal amounts of protein or medium were resolved by 12% or 15% SDS-PAGE and ASIP was detected using an ASIP antibody (PA5-77052, Invitrogen, 1:1,000 dilution). Equal loading was confirmed by detection of β-actin using a β-actin antibody (ab8227, Abcam, 1:1,000 dilution).

### Melanocortin receptor signaling by cAMP assay

A Chinese hamster ovary cell line CHO-K1 (ATCC CCL-61) was grown in DMEM/F-12 supplemented with 10% FBS, 100 U ml<sup>-1</sup> penicillin and 100 µg ml<sup>-1</sup> streptomycin. Cells were at seeded at 0.9 × 10<sup>6</sup> cells per 25-cm<sup>2</sup> flask and transfected with plasmid (3 µg total amount of DNA) and Lipofectamine 2000 (Thermo Fisher Scientific). Plasmids encoding human MC1R<sup>61</sup>, human MC4R<sup>62</sup> and empty vector pcDps have previously been described.

One day after transfection, cells were split into 96-well plates (2 × 10<sup>4</sup> cells per well) and serum-starved for 16 h before the experiment. cAMP content of cell extracts was determined by a non-radioactive assay with ALPHAScreen (PerkinElmer) technology as previously described<sup>63</sup>. In brief, stimulation with various α-MSH (Sigma-Aldrich) concentrations in the absence or presence of 100 nM ASIP (R&D systems) or with various concentrations of ASIP alone were performed 48 h after transfection. Reactions were stopped by aspiration of medium and cells were lysed in 20 µl of lysis buffer containing 1 mM 3-isobutyl-1-methylxanthine. From each well, 5 µl of lysate were transferred to a 384-well plate. Acceptor beads and donor beads were added according to the manufacturers' protocol. Cyclic AMP accumulation data were analyzed using GraphPad Prism v.8.4.3.

### Screening for patients with *ASIP* mutations

In unselected cohorts of  $n = 1,745$  children of the Leipzig Childhood Obesity cohort (mean age, 11.6 years; female,  $n = 879$ ; male,  $n = 867$ ) as well as 2,051 children of healthy population childhood cohorts (Leipzig childhood cohort,  $n = 1,447$ ; mean age, 11.7 years; female,  $n = 755$ ; male,  $n = 692$ ; Leipzig Lifestyle and environmental factors and their Influence on Newborns Allergy risk (LINA) cohort<sup>64</sup>,  $n = 604$ ; mean age, 4 years; female,  $n = 291$ ; male,  $n = 313$ ) we screened for carriers of the genomic *ITCH-ASIP* fusion. The studies were approved by the ethics committee of the University of Leipzig (Leipzig childhood cohort, reg. nos. 007-04/027-04, 782-1998, and 029-2006; LINA cohort, reg. nos. 046-2006 and 144-10-31052010, registered in <https://www.birthcohorts.net> since 6 May 2019). Children from the age of 12 years on and their guardians provided informed consent. Twenty patients with obesity and red hair color, who were previously suspected for mutations in the *POMC* gene were additionally screened for genomic *ITCH-ASIP* fusion. These patients were recruited at the Freie Universität Berlin, Humboldt-Universität zu Berlin, Institute for Experimental Pediatric Endocrinology (mean age, 9.4 years; female,  $n = 13$ ; male,  $n = 7$ ). This analysis was approved by the local ethical committee (EA2/131/11).

gDNA copy numbers of the *ITCH-ASIP* fusion sequence were quantified using SYBR green qRT-PCR using the Maxima SYBR Green/ROX qPCR Master Mix (2×) (Thermo Fisher Scientific) and the *ITCH-ASIP* fusion primers (Supplementary Appendix and Supplementary Table 5) with an input of 2–10 ng gDNA per reaction. Copy numbers were normalized to copy numbers of β-actin. On each plate, samples from the patient were carried along as a positive control.

For comparison of BMI SDS and height SDS of identified carriers with *ASIP* mutation with the obesity cohort, we excluded eight patients with underlying syndromic or endocrine diseases (Prader-Willi

syndrome, growth hormone deficiency, syndromic short stature or autoimmune polyendocrinopathy) and a further three patients had missing data for either height or BMI. Of the LINA birth cohort, from  $n = 183$  probands, data and samples were only available at birth and were, therefore, excluded from comparative anthropometric analyses.

### Statistical analyses

If not otherwise stated, statistical analyses were performed using a Student's  $t$ -test (two-sided) in GraphPad Prism 6 (GraphPad Software).  $P$  values  $< 0.05$  were considered statistically significant.

### Reporting summary

Further information on research design is available in the Nature Portfolio Reporting Summary linked to this article.

### Data availability

The datasets generated during and/or analyzed during the current study are deposited as source files except for patient individualized datasets that underly patient confidentiality restrictions but are available from the corresponding author upon reasonable request. Source data are provided with this paper.

### References

- Bouchard, C. Genetics of obesity: what we have learned over decades of research. *Obesity* **29**, 802–820. (2021).
- Hinney, A., Körner, A. & Fischer-Posovszky, P. The promise of new anti-obesity therapies arising from knowledge of genetic obesity traits. *Nat. Rev. Endocrinol.* <https://doi.org/10.1038/s41574-022-00716-0> (2022).
- Lotta, L. A. et al. Human gain-of-function MC4R variants show signaling bias and protect against obesity. *Cell* **177**, 597–607 (2019).
- van der Klaauw, A. A. & Farooqi, I. S. The hunger genes: pathways to obesity. *Cell* **161**, 119–132. (2015).
- Wabitsch, M. et al. Measurement of immunofunctional leptin to detect and monitor patients with functional leptin deficiency. *Eur. J. Endocrinol.* **176**, 315–322. (2017).
- Marenne, G. et al. Exome sequencing identifies genes and gene sets contributing to severe childhood obesity, linking PHIP variants to repressed POMC transcription. *Cell Metab.* **31**, 1107–1119 (2020).
- Clément, K. et al. Efficacy and safety of setmelanotide, an MC4R agonist, in individuals with severe obesity due to LEPR or POMC deficiency: single-arm, open-label, multicentre, phase 3 trials. *Lancet Diabetes Endocrinol.* **8**, 960–970. (2020).
- Ericson, M. D., Freeman, K. T., Schnell, S. M., Fleming, K. A. & Haskell-Luevano, C. Structure-activity relationship studies on a macrocyclic agouti-related protein (AGRP) scaffold reveal agouti signaling protein (ASP) residue substitutions maintain melanocortin-4 receptor antagonist potency and result in inverse agonist pharmacology at the melanocortin-5 receptor. *J. Med. Chem.* **60**, 8103–8114. (2017).
- Duhl, D. M., Vrieling, H., Miller, K. A., Wolff, G. L. & Barsh, G. S. Neomorphic agouti mutations in obese yellow mice. *Nat. Genet.* **8**, 59–65 (1994).
- Klebig, M. L., Wilkinson, J. E., Geisler, J. G. & Woychik, R. P. Ectopic expression of the agouti gene in transgenic mice causes obesity, features of type II diabetes, and yellow fur. *Proc. Natl Acad. Sci. USA* **92**, 4728–4732 (1995).
- Miltenberger, R. J., Mynatt, R. L., Wilkinson, J. E. & Woychik, R. P. The role of the agouti gene in the yellow obese syndrome. *J. Nutr.* **127**, 1902S–1907SS (1997).
- Moussa, N. M. & Claycombe, K. J. The yellow mouse obesity syndrome and mechanisms of agouti-induced obesity. *Obes. Res.* **7**, 506–514 (1999).
- Wabitsch, M. et al. Characterization of a human preadipocyte cell strain with high capacity for adipose differentiation. *Int. J. Obes. Relat. Metab. Disord.* **25**, 8–15 (2001).
- Morgan, M. D. et al. Genome-wide study of hair colour in UK Biobank explains most of the SNP heritability. *Nat. Commun.* **9**, 5271 (2018).
- Kempf, E. et al. Dynamic alterations in linear growth and endocrine parameters in children with obesity and height reference values. *eClinicalMedicine* **37**, 100977 (2021).
- Kwon, H. Y. et al. Molecular structure and chromosomal mapping of the human homolog of the agouti gene. *Proc. Natl Acad. Sci. USA* **91**, 9760–9764 (1994).
- Yang, Y.-K. et al. Effects of recombinant agouti-signaling protein on melanocortin action. *Mol. Endocrinol.* **11**, 274–280 (1997).
- Voisey, J., Imbeault, P., Hutley, L., Prins, J. B. & van Daal, A. Body mass index-related human adipocyte agouti expression is sex-specific but not depot-specific. *Obes. Res.* **10**, 447–452 (2002).
- Landgraf, K. et al. Evidence of early alterations in adipose tissue biology and function and its association with obesity-related inflammation and insulin resistance in children. *Diabetes* **64**, 1249–1261 (2015).
- Patel, M. P. et al. Loop-swapped chimeras of the agouti-related protein and the agouti signaling protein identify contacts required for melanocortin 1 receptor selectivity and antagonism. *J. Mol. Biol.* **404**, 45–55 (2010).
- He, Z. et al. Direct and indirect effects of liraglutide on hypothalamic POMC and NPY/AGRP neurons - Implications for energy balance and glucose control. *Mol. Metab.* **28**, 120–134. (2019).
- Voisey, J. & Van Daal, A. Agouti: from mouse to man, from skin to fat. *Pigment Cell Res.* **15**, 10–18 (2002).
- Small, C. J. et al. Chronic CNS administration of agouti-related protein (AGRP) reduces energy expenditure. *Int. J. Obes. Relat. Metab. Disord.* **27**, 530–533 (2003).
- Tang-Christensen, M. et al. Central administration of ghrelin and agouti-related protein (83-132) increases food intake and decreases spontaneous locomotor activity in rats. *Endocrinology* **145**, 4645–4652 (2004).
- Cavalcanti-de-Albuquerque, J. P., Bober, J., Zimmer, M. R. & Dietrich, M. O. Regulation of substrate utilization and adiposity by AGRP neurons. *Nat. Commun.* **10**, 311 (2019).
- Lubrano-Berthelmer, C. et al. Melanocortin 4 receptor mutations in a large cohort of severely obese adults: prevalence, functional classification, genotype-phenotype relationship, and lack of association with binge eating. *J. Clin. Endocrinol. Metab.* **91**, 1811–1818 (2006).
- Winkler, T. W. et al. The influence of age and sex on genetic associations with adult body size and shape: a large-scale genome-wide interaction study. *PLoS Genet.* **11**, e1005378 (2015).
- Mynatt, R. L. & Stephens, J. M. Regulation of PPAR $\gamma$  and obesity by agouti/melanocortin signaling in adipocytes. *Ann. NY Acad. Sci.* **994**, 141–146 (2003).
- Schnabl, K., Westermeier, J., Li, Y. & Klingenspor, M. Opposing actions of adrenocorticotrophic hormone and glucocorticoids on UCP1-mediated respiration in brown adipocytes. *Front. Physiol.* **9**, 1931 (2018).
- Yang, C. H. et al. Independent phenotypic plasticity axes define distinct obesity sub-types. *Nat. Metab.* **4**, 1150–1165. (2022).
- Inge, T. H. et al. Five-year outcomes of gastric bypass in adolescents as compared with adults. *The. N. Engl. J. Med.* **380**, 2136–2145. (2019).
- Nakayama, K. & Ishida, T. Alu-mediated 100-kb deletion in the primate genome: the loss of the agouti signaling protein gene in the lesser apes. *Genome Res* **16**, 485–490 (2006).

33. Chandramohan, B., Renieri, C., La Manna, V., La & Terza, A. The alpaca agouti gene: genomic locus, transcripts and causative mutations of eumelanin and pheomelanin coat color. *Gene* **521**, 303–310 (2013).
34. Girardot, M. et al. The insertion of a full-length *Bos taurus* LINE element is responsible for a transcriptional deregulation of the Normande Agouti gene. *Pigment Cell Res.* **19**, 346–355 (2006).
35. Norris, B. J. & Whan, V. A. A gene duplication affecting expression of the ovine ASIP gene is responsible for white and black sheep. *Genome Res.* **18**, 1282–1293 (2008).
36. Robic, A. et al. Two new structural mutations in the 5' region of the ASIP gene cause diluted feather color phenotypes in Japanese quail. *Genet Sel. Evol.* **51**, 12 (2019).
37. Wade, K. H. et al. Loss-of-function mutations in the melanocortin 4 receptor in a UK birth cohort. *Nat. Med.* **27**, 1088–1096. (2021).
38. Taylor, N. J. et al. Inherited variation at MC1R and ASIP and association with melanoma-specific survival. *Int. J. Cancer* **136**, 2659–2667 (2015).
39. Iepsen, E. W. et al. Patients with obesity caused by melanocortin-4 receptor mutations can be treated with a glucagon-like peptide-1 receptor agonist. *Cell Metab.* **28**, 23–32 (2018).
40. Kromeyer-Hauschild, K. et al. Percentiles of body mass index in children and adolescents evaluated from different regional German studies. *Monatsschr. Kinder* **149**, 807–18. (2001).
41. AWMF. Evidence-based (S3) Guideline of the Working Group on Childhood and Adolescent Obesity (AGA) of the German Obesity Society (DAG) and the German Society of Pediatrics and Adolescent Medicine (DGKJ). <https://awmf.org/leitlinien/detail/ll/050-002.html> (2019).
42. Hilbert, A. & Tuschen-Caffier, B. *Eating Disorder Examination-Questionnaire: Deutschsprachige Übersetzung* (Verlag für Psychotherapie, 2006).
43. Fairburn, C. G. *Cognitive Behavior Therapy and Eating Disorders* (Guilford Publications, 2008).
44. Hilbert, A., de Zwaan, M. & Braehler, E. How frequent are eating disturbances in the population? Norms of the eating disorder examination-questionnaire. *PLoS ONE* **7**, e29125 (2012).
45. Nagl, M., Hilbert, A., de Zwaan, M., Braehler, E. & Kersting, A. The German version of the Dutch Eating Behavior Questionnaire: psychometric properties, measurement invariance, and population-based norms. *PLoS ONE* **11**, e0162510 (2016).
46. Landgraf, K. et al. The obesity-susceptibility gene TMEM18 promotes adipogenesis through activation of PPARγ. *Cell Rep.* <https://doi.org/10.1016/j.celrep.2020.108295> (2020).
47. Doubling Time Computing. <http://www.doubling-time.com/compute.php> (2006).
48. Bernhard, F. et al. Functional relevance of genes implicated by obesity genome-wide association study signals for human adipocyte biology. *Diabetologia* **56**, 311–322 (2013).
49. Smyth, G., Thorne, N. & Wettenhall, J. limma: Linear models for microarray data user's guide. *Bioinformatics and computational biology solutions using R and bioconductor2011*.
50. Langmead, B., Trapnell, C., Pop, M. & Salzberg, S. L. Ultrafast and memory-efficient alignment of short DNA sequences to the human genome. *Genome Biol.* **10**, R25 (2009).
51. Li, H. et al. The Sequence Alignment/Map format and SAMtools. *Bioinformatics* **25**, 2078–2079 (2009).
52. Pertea, M., Kim, D., Pertea, G. M., Leek, J. T. & Salzberg, S. L. Transcript-level expression analysis of RNA-seq experiments with HISAT, StringTie and Ballgown. *Nat. Protoc.* **11**, 1650–1667 (2016).
53. Pertea, M. et al. StringTie enables improved reconstruction of a transcriptome from RNA-seq reads. *Nat. Biotechnol.* **33**, 290–295 (2015).
54. Robinson, J. T. et al. Integrative genomics viewer. *Nat. Biotechnol.* **29**, 24–26 (2011).
55. Thorvaldsdóttir, H., Robinson, J. T. & Mesirov, J. P. Integrative Genomics Viewer (IGV): high-performance genomics data visualization and exploration. *Brief. Bioinform.* **14**, 178–192 (2013).
56. Eberherr, A. C. et al. Rescue of STAT3 function in hyper-IgE syndrome using adenine base editing. *CRISPR J.* **4**, 178–190. (2021).
57. Shi, Y., Kirwan, P. & Livesey, F. J. Directed differentiation of human pluripotent stem cells to cerebral cortex neurons and neural networks. *Nat. Protoc.* **7**, 1836–1846 (2012).
58. Borchin, B., Chen, J. & Barberi, T. Derivation and FACS-mediated purification of PAX3<sup>+</sup>/PAX7<sup>+</sup> skeletal muscle precursors from human pluripotent stem cells. *Stem Cell Rep.* **1**, 620–631 (2013).
59. Ori, C. et al. Single cell trajectory analysis of human pluripotent stem cells differentiating towards lung and hepatocyte progenitors. Preprint at *bioRxiv* <https://doi.org/10.1101/2021.02.23.432413> (2021).
60. Wang, L., Egli, D. & Leibel, R. L. Efficient generation of hypothalamic neurons from human pluripotent stem cells. *Curr. Protoc. Hum. Genet.* **90**, 21.5.1–21.5.14 (2016).
61. Lalueza-Fox, C. et al. A melanocortin 1 receptor allele suggests varying pigmentation among Neanderthals. *Science* **318**, 1453–1455 (2007).
62. Stäubert, C. et al. Evolutionary aspects in evaluating mutations in the melanocortin 4 receptor. *Endocrinology* **148**, 4642–4648 (2007).
63. Peters, A. et al. Natural biased signaling of hydroxycarboxylic acid receptor 3 and G protein-coupled receptor 84. *Cell Commun. Signal.* **18**, 31 (2020).
64. Hinz, D. et al. Cord blood T<sub>reg</sub>s with stable FOXP3 expression are influenced by prenatal environment and associated with atopic dermatitis at the age of one year. *Allergy* **67**, 380–389 (2012).
65. American Diabetes Association. 2. Classification and diagnosis of diabetes: standards of medical care in diabetes-2020. *Diabetes Care* **43**, S14–S31 (2020).
66. Bussler, S. et al. New pediatric percentiles of liver enzyme serum levels (alanine aminotransferase, aspartate aminotransferase, γ-glutamyltransferase): effects of age, sex, body mass index, and pubertal stage. *Hepatology* **68**, 1319–1330 (2018).

## Acknowledgements

We thank the children and parents who participated in the study, the physicians and technical and clinical assistants who helped with the study and U. Stenzel for the bioinformatic transcript analyses. We also thank E. Rusha and A. Pertek from the iPSC Core Facility, Institute of Stem Cell Research, Helmholtz Zentrum München for generating iPSCs. We thank A.-D. Liebing from the Rudolf Schönheimer Institute of Biochemistry for technical support. We thank H. Schiffmann for his support with the collection of patient data. This work was supported by the German Research Foundation for the Clinical Research Center 'Obesity Mechanisms' SFB1052/CRC1052 (no. 209933838) projects C05 to A. Körner, C09 to A. Körner and K.L., and KO3512/3-1 to A. Körner and E.Z., and by the German Diabetes Association to A. Körner. R.S. was funded by the joint Clinician Scientist Program of the Medical Faculty and the Helmholtz Institute for Metabolic, Obesity and Vascular Research of the Helmholtz Zentrum München at the University of Leipzig. The funders of the study had no role in the study design, in the collection, analysis and interpretation of data or in the writing of the report.

## Author contributions

A. Körner was the project principal investigator and led the design of the study, established the project and funding and supervised experiments, analyses and data interpretation. A. Körner assumes responsibility for the completeness and integrity of the data and the fidelity of the report. W.K. contributed to discussion of manuscript.

E.K., K.L., R.S., M.H., A.H., R.A.J., P.B., A. Kühnapfel, Y.H.T., C.S., T.S., W.R., E.Z. and A. Körner performed and supervised experiments, performed clinical assessments, data analyses and interpretation and drafted the manuscript. G.H. and P.K. provided cohort samples for mutation screening. M.B. contributed to project management, data discussions and edited the manuscript. All authors contributed to the interpretation of study findings and had the opportunity to review and revise the final manuscript.

### Competing interests

The authors declare no competing interests.

### Additional information

**Extended data** is available for this paper at <https://doi.org/10.1038/s42255-022-00703-9>.

**Supplementary information** The online version contains supplementary material available at <https://doi.org/10.1038/s42255-022-00703-9>.

**Correspondence and requests for materials** should be addressed to Antje Körner.

**Peer review information** *Nature Metabolism* thanks the anonymous reviewers for their contribution to the peer review of this work.

Primary Handling Editor: Christoph Schmitt, in collaboration with the *Nature Metabolism* team.

**Reprints and permissions information** is available at [www.nature.com/reprints](http://www.nature.com/reprints).

**Publisher's note** Springer Nature remains neutral with regard to jurisdictional claims in published maps and institutional affiliations.

**Open Access** This article is licensed under a Creative Commons Attribution 4.0 International License, which permits use, sharing, adaptation, distribution and reproduction in any medium or format, as long as you give appropriate credit to the original author(s) and the source, provide a link to the Creative Commons license, and indicate if changes were made. The images or other third party material in this article are included in the article's Creative Commons license, unless indicated otherwise in a credit line to the material. If material is not included in the article's Creative Commons license and your intended use is not permitted by statutory regulation or exceeds the permitted use, you will need to obtain permission directly from the copyright holder. To view a copy of this license, visit <http://creativecommons.org/licenses/by/4.0/>.

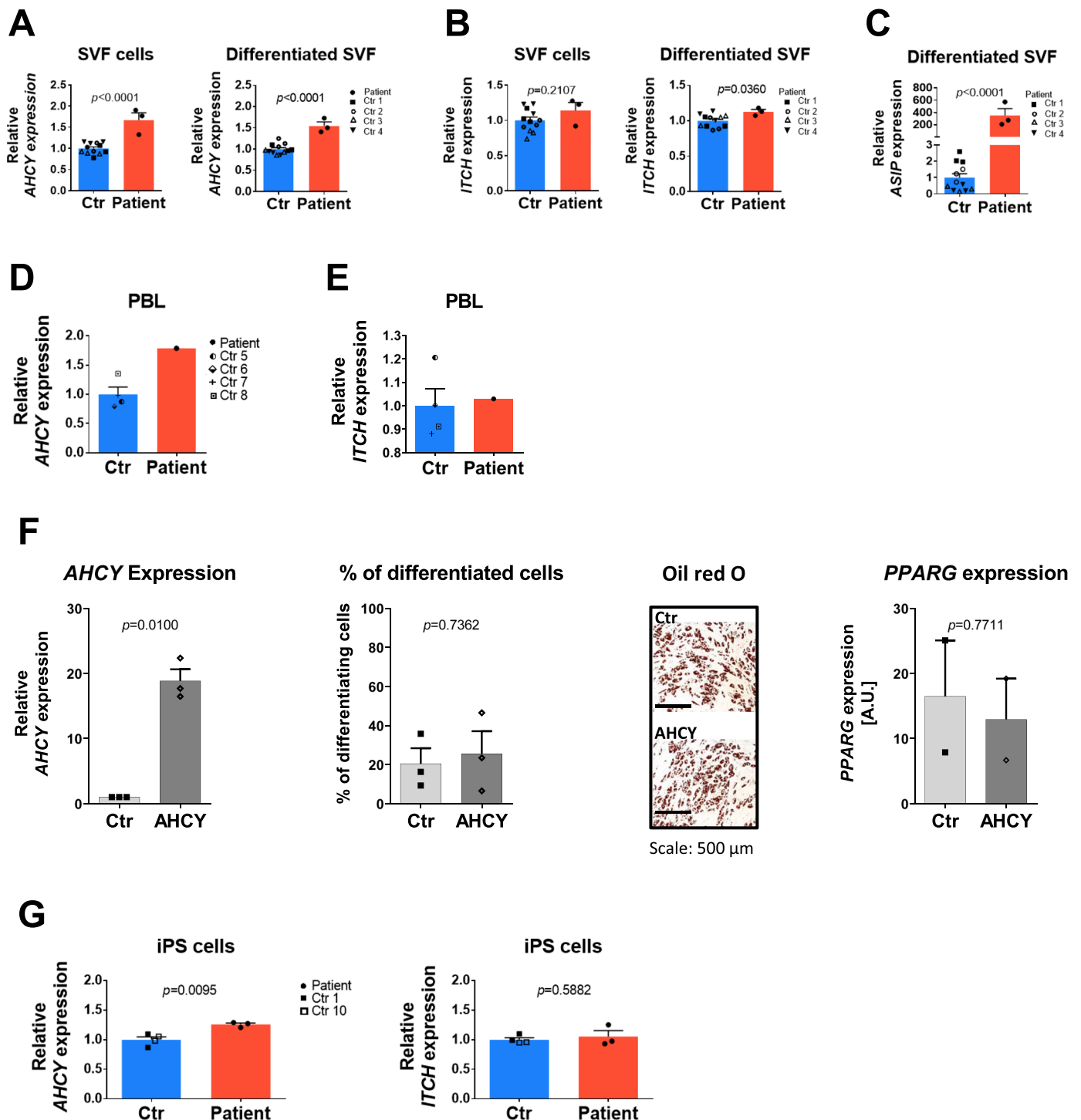
© The Author(s) 2022

<sup>1</sup>University Hospital for Children and Adolescents, Center for Pediatric Research, Medical Faculty, University of Leipzig, Leipzig, Germany.

<sup>2</sup>Helmholtz Institute for Metabolic Obesity and Vascular Research (HI-MAG) of the Helmholtz Zentrum München at the University of Leipzig and University Hospital Leipzig, Leipzig, Germany. <sup>3</sup>Department of Psychosomatic Medicine and Psychotherapy, Medical Faculty, University of Leipzig, Leipzig, Germany.

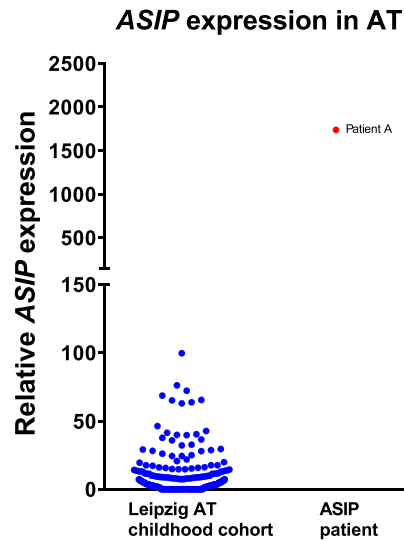
<sup>4</sup>University Medical Center Leipzig, Institute of Human Genetics, Medical Faculty, University of Leipzig, Leipzig, Germany. <sup>5</sup>Department of Environmental Immunology, Helmholtz Centre for Environmental Research-UFZ, Leipzig, Germany. <sup>6</sup>Institute for Medical Informatics, Statistics and Epidemiology, Medical Faculty, University of Leipzig, Leipzig, Germany. <sup>7</sup>Section on Integrative Physiology and Metabolism, Joslin Diabetes Center, Harvard Medical School, Boston, MA, USA. <sup>8</sup>Division of Molecular Biochemistry, Rudolf Schönheimer Institute of Biochemistry, Medical Faculty, University of Leipzig, Leipzig, Germany. <sup>9</sup>Institute for Experimental Pediatric Endocrinology, Charité Universitätsmedizin Berlin, Corporate Member of Freie Universität Berlin, Humboldt-Universität zu Berlin, Berlin, Germany. <sup>10</sup>Institute of Translational Genomics, Helmholtz Zentrum München - German Research Center for Environmental Health, Neuherberg, Germany. <sup>11</sup>TUM School of Medicine, Translational Genomics, Technical University of Munich and Klinikum Rechts der Isar, Munich, Germany. <sup>12</sup>LIFE-Leipzig Research Center for Civilization Diseases, Medical Faculty, University of Leipzig, Leipzig, Germany. <sup>13</sup>Medical Department III-Endocrinology, Nephrology, Rheumatology, University of Leipzig, Leipzig, Germany. <sup>14</sup>These authors contributed equally: Elena Kempf, Kathrin Landgraf. ✉e-mail: [antje.koerner@medizin.uni-leipzig.de](mailto:antje.koerner@medizin.uni-leipzig.de)





**Extended Data Fig. 1 | *AHCY* overexpression in different cell types.** Gene expression levels of (A) adenosylhomocysteinase (*AHCY*) and (B) itchy E3 ubiquitin protein ligase (*ITCH*) in stromal vascular fraction (SVF) cells before and after adipocyte differentiation and compared to that of (C) agouti signaling protein (*ASIP*) in differentiated SVF cells are shown from the patient and controls (Ctr) patients 1-4 (n=4; 3 females, 1 male) matched for age (mean age 13.8 years) and body weight state (all presenting with overweight or obesity). Data points of n=3 independent experiments are indicated for each subject. In peripheral blood leukocytes (PBL) *AHCY* (D) and *ITCH* (E) expression are shown from the patient and controls. Data points are indicated for each subject. (F) Relative *AHCY* expression in Simpson–Golabi–Behmel syndrome (SGBS) cells after transfection with pCMV-Entry control vector (Ctr) or pCMV-AHCY (AHCY) in n=3 independent experiments. Transfected SGBS cells were differentiated into adipocytes and the percentage of differentiated cells was determined by cell counting after

Hoechst and Nile red staining. Using the same cells adipogenic capacity was compared by Oil red O staining (representative microscopic pictures from one of three independent experiments; scale bar = 500  $\mu\text{m}$ ) and gene expression of the adipogenic marker gene peroxisome proliferator-activated receptor gamma (*PPARG*) after differentiation in n=2 independent experiments. Bar plots show the mean  $\pm$  SEM. (G) *AHCY* and *ITCH* expression levels are shown for SVF cell-derived pluripotent stem cells (iPSCs) from three clones of the patient and two clones from each of the control (Ctr) children, 1 and 10. Data points for each clone from each subject are indicated. The bar plots A-E and G present the mean values  $\pm$  SEM as a fold change of the controls. Gene expression data were normalized to the expression of  $\beta$ -actin and TATA-box-binding protein. All bars from controls are shown in blue and from the patient in red. *P* values derived using two-sided Student's *t*-test are given.



**Extended Data Fig. 2 | ASIP expression in adipose tissue samples of children.** Gene expression levels of agouti signaling protein (*ASIP*) in subcutaneous adipose tissue (AT) of 328 children included in the Leipzig AT childhood cohort are shown in comparison to patient A. Data points are indicated for each subject. Gene

expression data were normalized to the expression of  $\beta$ -actin, TATA-box-binding protein and hypoxanthine-guanine-phosphoribosyltransferase. Data points from controls are shown in blue and from the patient in red.

## Reporting Summary

Nature Research wishes to improve the reproducibility of the work that we publish. This form provides structure for consistency and transparency in reporting. For further information on Nature Research policies, see our [Editorial Policies](#) and the [Editorial Policy Checklist](#).

### Statistics

For all statistical analyses, confirm that the following items are present in the figure legend, table legend, main text, or Methods section.

n/a Confirmed

- The exact sample size ( $n$ ) for each experimental group/condition, given as a discrete number and unit of measurement
- A statement on whether measurements were taken from distinct samples or whether the same sample was measured repeatedly
- The statistical test(s) used AND whether they are one- or two-sided  
*Only common tests should be described solely by name; describe more complex techniques in the Methods section.*
- A description of all covariates tested
- A description of any assumptions or corrections, such as tests of normality and adjustment for multiple comparisons
- A full description of the statistical parameters including central tendency (e.g. means) or other basic estimates (e.g. regression coefficient) AND variation (e.g. standard deviation) or associated estimates of uncertainty (e.g. confidence intervals)
- For null hypothesis testing, the test statistic (e.g.  $F$ ,  $t$ ,  $r$ ) with confidence intervals, effect sizes, degrees of freedom and  $P$  value noted  
*Give  $P$  values as exact values whenever suitable.*
- For Bayesian analysis, information on the choice of priors and Markov chain Monte Carlo settings
- For hierarchical and complex designs, identification of the appropriate level for tests and full reporting of outcomes
- Estimates of effect sizes (e.g. Cohen's  $d$ , Pearson's  $r$ ), indicating how they were calculated

*Our web collection on [statistics for biologists](#) contains articles on many of the points above.*

### Software and code

Policy information about [availability of computer code](#)

#### Data collection

Resting energy expenditure of the patient was measured using an indirect calorimeter (Quark RMR, Cosmed Germany). Absorbance and fluorescence of cell were analyzed using the BZ-8000 microscope (Keyence, Neu-Isenburg, Germany). Mitochondrial function was assessed using the Seahorse XFe24 Analyzer (Agilent Technologies). Transcriptome-wide gene expression was measured using a HumanHT-12 v4 BeadChip array (ILLUMINA) by the Core Unit for DNA technologies of the University Hospital Leipzig. TaqMan quantitative real-time polymerase chain reaction (qRT-PCR) was performed using the QuantStudio3 or QuantStudio6 Real-Time PCR System (Applied Biosystems®). RNA quantity was measured with a spectrometer (Nanodrop ND 1000). RNA quality was analyzed on the Agilent 2100 bioanalyzer using the RNA 6000 Nano Chip (Agilent Technologies, USA). For whole genome sequencing the DNA libraries were quantified by qPCR (LightCycler 480, Roche) and the Fragment Analyzer (Agilent). Libraries were sequenced paired end 2 x 150 bp to a coverage > 38x on a NovaSeq 6000 (ILLUMINA). cDNA libraries for RNA sequencing were on the Illumina HiScanSQ Sequencing System (Fa Macrogen Europe). Luciferase activities were measured using a CLARIOstar plate reader (BMG Labtech).

## Data analysis

If not otherwise stated, statistical analyses were performed using Student's t-test (two-sided) in GraphPad Prism 6 (GraphPad Software, San Diego, CA, version 6.07).  
 For RNA sequencing reads were mapped to the reference human genome (GRCh38.p13 (Genome Reference Consortium Human Build 38), INSDC Assembly GCA\_000001405.28, Dec 2013) using Tophat. After indexing with samtools the mapped reads were assembled to transcripts and quantified by StringTie.  
 For whole genome sequencing bioinformatic analysis was performed using the ILLUMINA DRAGEN pipeline (07.021.595.3.7.5).  
 TruSight One Sequencing panel were analysed using the software Varis and Varfeed CNV (Limbus, Rostock).  
 Molecular karyotyping of genomic DNA has been analysed using BlueFuse Multi (version 4.4).  
 Cyclic AMP accumulation data from the ALPHAScreen cAMP assay were analysed using GraphPad Prism version 8.4.3.

For manuscripts utilizing custom algorithms or software that are central to the research but not yet described in published literature, software must be made available to editors and reviewers. We strongly encourage code deposition in a community repository (e.g. GitHub). See the Nature Research [guidelines for submitting code & software](#) for further information.

## Data

Policy information about [availability of data](#)

All manuscripts must include a [data availability statement](#). This statement should provide the following information, where applicable:

- Accession codes, unique identifiers, or web links for publicly available datasets
- A list of figures that have associated raw data
- A description of any restrictions on data availability

The datasets generated during and/or analysed during the current study are deposited as source files except for patient individualized data sets that underly patient confidentiality restrictions but are available from the corresponding author upon reasonable request. Statistical source data files of the displayed graphs are provided in separate Excel files. Unprocessed immunoblots and agarose gels are provided as source data.

We have provided the doi of the R-code for transcriptomic analyses corresponding to figure (<https://doi.org/10.5281/zenodo.7223530>). The data set is available upon request as it contains ~omic and, therefore, patient sensitive information.

The same applies to WGS and WES data these we will provide upon request due to data protection issues.

From RNAseq data of the patient and controls we exclusively and targetedly extracted the expression information on the genes ASIP, ITCH and AHCY. These data are directly given in supplementary Table S2. Hence, it is not a "classical RNA seq analysis".

## Field-specific reporting

Please select the one below that is the best fit for your research. If you are not sure, read the appropriate sections before making your selection.

Life sciences       Behavioural & social sciences       Ecological, evolutionary & environmental sciences

For a reference copy of the document with all sections, see [nature.com/documents/nr-reporting-summary-flat.pdf](https://www.nature.com/documents/nr-reporting-summary-flat.pdf)

## Life sciences study design

All studies must disclose on these points even when the disclosure is negative.

Sample size	No sample size determination was performed. The manuscript is a case report of a newly identified patient with obesity and novel monogenic mutation in the ASIP gene locus.
Data exclusions	No data was excluded from the study.
Replication	Reproducibility of findings was verified using biological replicates and independent experiments and all exact n values were indicated in figure legends.
Randomization	Randomization was not performed in this study. The manuscript is a case report of a newly identified patient with obesity and novel monogenic mutation in the ASIP gene locus. Wherever possible control patients were matched for age and sex. Details of control patients and control cohorts are given in supplementary table S1 or the respective figure legends.
Blinding	Blinding was not performed in this study. The manuscript is a case report of a newly identified patient with obesity and novel monogenic mutation in the ASIP gene locus. For experimental analyses results were confirmed in several independent experiments. Data collection in cohorts occurred not in the scope of this study but before and therefore were blinded.

## Reporting for specific materials, systems and methods

We require information from authors about some types of materials, experimental systems and methods used in many studies. Here, indicate whether each material, system or method listed is relevant to your study. If you are not sure if a list item applies to your research, read the appropriate section before selecting a response.

## Materials & experimental systems

## Methods

- n/a  Involved in the study
- Antibodies
- Eukaryotic cell lines
- Palaeontology and archaeology
- Animals and other organisms
- Human research participants
- Clinical data
- Dual use research of concern

- n/a  Involved in the study
- ChIP-seq
- Flow cytometry
- MRI-based neuroimaging

## Antibodies

Antibodies used	anti-ASIP antibody (PA5-77052, Invitrogen, dilution 1:1000); anti- $\beta$ -actin antibody (ab8227, Abcam, dilution 1:1000)
Validation	Antibodies have been tested by the companies according to their website: Anti-ASIP antibody: <a href="https://www.abcam.com/beta-actin-antibody-ab8227.html">https://www.abcam.com/beta-actin-antibody-ab8227.html</a> Furthermore, specificity was verified by including positive controls (recombinant ASIP protein), by verifying expected protein size and by performing ASIP knockdown experiments. Anti-beta Actin: <a href="https://www.abcam.com/beta-actin-antibody-ab8227.html">https://www.abcam.com/beta-actin-antibody-ab8227.html</a>

## Eukaryotic cell lines

Policy information about [cell lines](#)

Cell line source(s)	Human embryo kidney cell line 293 (HEK293) (Sigma-Aldrich, ECACC 85120602), Chinese hamster ovary cell line CHO-K1 (ATCC CCL-61™), Human preadipocyte cell line from a patient with Simpson–Golabi–Behmel syndrome (SGBS) provided by Martin Wabitsch (University of Ulm, Germany) induced pluripotent stem cell lines: HMGU1 and SVF derived iPSCs (iPSC Core Facility, Helmholtz Zentrum München)
Authentication	None of the cell lines were authenticated.
Mycoplasma contamination	Cell lines were negative for Mycoplasma contamination.
Commonly misidentified lines (See <a href="#">ICLAC</a> register)	No commonly misidentified cell lines were used in this study.

## Human research participants

Policy information about [studies involving human research participants](#)

Population characteristics	Detailed characteristics of the study participants are given in the "Case Report" section for the index patient and her father and in the Supplementary Appendix, Table S1 for the control patients. Population characteristics of the control cohorts are provided in the methods section.
Recruitment	The index patient and children of the control group were participants in the Leipzig Adipose Tissue Childhood30 (NCT02208141) and the Leipzig Obesity Childhood (NCT04491344) cohorts. Control cohorts for obesity were recruited from the outpatient clinic of the university hospital Leipzig and Berlin, lean controls were recruited from the area around Leipzig.
Ethics oversight	Ethics Committee of the University of Leipzig (reg. no. 007-04/027-04, reg. no. 782-1998, reg. no. 029-2006; reg. no. 046-2006, reg. no. 144-10-31052010), Ethics Committee of the Charité – Universitätsmedizin Berlin (EA2/131/11)

Note that full information on the approval of the study protocol must also be provided in the manuscript.

## Clinical data

Policy information about [clinical studies](#)

All manuscripts should comply with the ICMJE [guidelines for publication of clinical research](#) and a completed [CONSORT checklist](#) must be included with all submissions.

Clinical trial registration	Leipzig Adipose Tissue Childhood cohort: NCT02208141, Leipzig Obesity Childhood cohort: NCT04491344
Study protocol	Trial protocol can be assessed with the National Clinical Trials accession numbers.
Data collection	Data of the patient were collected between 2005 and now in regular intervals.

The manuscript is a case report of a newly identified patient with obesity and novel monogenic mutation in the ASIP gene locus. Outcomes were diagnostic and obesity-related parameters.